IJOER

RESEARCH JOURNAL

ISSN

2395-6992

International Journal of Engineering Research & Science

www.ijoer.com

www.adpublications.org

Volume-5! Issue-10! October, 2019 www.ijoer.com ! info@ijoer.com

Preface

We would like to present, with great pleasure, the inaugural volume-5, Issue-10, October 2019, of a scholarly journal, *International Journal of Engineering Research & Science*. This journal is part of the AD Publications series *in the field of Engineering, Mathematics, Physics, Chemistry and science Research Development*, and is devoted to the gamut of Engineering and Science issues, from theoretical aspects to application-dependent studies and the validation of emerging technologies.

This journal was envisioned and founded to represent the growing needs of Engineering and Science as an emerging and increasingly vital field, now widely recognized as an integral part of scientific and technical investigations. Its mission is to become a voice of the Engineering and Science community, addressing researchers and practitioners in below areas

Chemical Engineering	
Biomolecular Engineering	Materials Engineering
Molecular Engineering	Process Engineering
Corrosion Engineering	
Civil Engineering	
Environmental Engineering	Geotechnical Engineering
Structural Engineering	Mining Engineering
Transport Engineering	Water resources Engineering
Electrical Engineering	
Power System Engineering	Optical Engineering
Mechanical Engineering	
Acoustical Engineering	Manufacturing Engineering
Optomechanical Engineering	Thermal Engineering
Power plant Engineering	Energy Engineering
Sports Engineering	Vehicle Engineering
Software Engineering	
Computer-aided Engineering	Cryptographic Engineering
Teletraffic Engineering	Web Engineering
System Engineering	
Mathematics	
Arithmetic	Algebra
Number theory	Field theory and polynomials
Analysis	Combinatorics
Geometry and topology	Topology
Probability and Statistics	Computational Science
Physical Science	Operational Research
Physics	
Nuclear and particle physics	Atomic, molecular, and optical physics
Condensed matter physics	Astrophysics
Applied Physics	Modern physics
Philosophy	Core theories

Chemistry	
Analytical chemistry	Biochemistry
Inorganic chemistry	Materials chemistry
Neurochemistry	Nuclear chemistry
Organic chemistry	Physical chemistry
Other Engineering Areas	
Aerospace Engineering	Agricultural Engineering
Applied Engineering	Biomedical Engineering
Biological Engineering	Building services Engineering
Energy Engineering	Railway Engineering
Industrial Engineering	Mechatronics Engineering
Management Engineering	Military Engineering
Petroleum Engineering	Nuclear Engineering
Textile Engineering	Nano Engineering
Algorithm and Computational Complexity	Artificial Intelligence
Electronics & Communication Engineering	Image Processing
Information Retrieval	Low Power VLSI Design
Neural Networks	Plastic Engineering

Each article in this issue provides an example of a concrete industrial application or a case study of the presented methodology to amplify the impact of the contribution. We are very thankful to everybody within that community who supported the idea of creating a new Research with IJOER. We are certain that this issue will be followed by many others, reporting new developments in the Engineering and Science field. This issue would not have been possible without the great support of the Reviewer, Editorial Board members and also with our Advisory Board Members, and we would like to express our sincere thanks to all of them. We would also like to express our gratitude to the editorial staff of AD Publications, who supported us at every stage of the project. It is our hope that this fine collection of articles will be a valuable resource for *IJOER* readers and will stimulate further research into the vibrant area of Engineering and Science Research.

Mukesh Arora

(Chief Editor)

Dr. Mohamed Abdel Fatah Ashabrawy Moustafa

PhD. in Computer Science - Faculty of Science - Suez Canal University University, 2010, Egypt.

Assistant Professor Computer Science, Prince Sattam bin AbdulAziz University ALkharj, KSA.

Dr. Heba Mahmoud Mohamed Afify

Ph.D degree of philosophy in Biomedical Engineering, Cairo University, Egypt worked as Assistant Professor at MTI University.

Dr. Aurora Angela Pisano

Ph.D. in Civil Engineering, Currently Serving as Associate Professor of Solid and Structural Mechanics (scientific discipline area nationally denoted as ICAR/08"–"Scienza delle Costruzioni"), University Mediterranea of Reggio Calabria, Italy.

Dr. Faizullah Mahar

Associate Professor in Department of Electrical Engineering, Balochistan University Engineering & Technology Khuzdar. He is PhD (Electronic Engineering) from IQRA University, Defense View,Karachi, Pakistan.

Dr. S. Kannadhasan

Ph.D (Smart Antennas), M.E (Communication Systems), M.B.A (Human Resources).

Dr. Christo Ananth

Ph.D. Co-operative Networks, M.E. Applied Electronics, B.E Electronics & Communication Engineering Working as Associate Professor, Lecturer and Faculty Advisor/ Department of Electronics & Communication Engineering in Francis Xavier Engineering College, Tirunelveli.

Dr. S.R.Boselin Prabhu

Ph.D, Wireless Sensor Networks, M.E. Network Engineering, Excellent Professional Achievement Award Winner from Society of Professional Engineers Biography Included in Marquis Who's Who in the World (Academic Year 2015 and 2016). Currently Serving as Assistant Professor in the department of ECE in SVS College of Engineering, Coimbatore.

Dr. Maheshwar Shrestha

Postdoctoral Research Fellow in DEPT. OF ELE ENGG & COMP SCI, SDSU, Brookings, SD Ph.D, M.Sc. in Electrical Engineering from SOUTH DAKOTA STATE UNIVERSITY, Brookings, SD.

Zairi Ismael Rizman

Senior Lecturer, Faculty of Electrical Engineering, Universiti Teknologi MARA (UiTM) (Terengganu) Malaysia Master (Science) in Microelectronics (2005), Universiti Kebangsaan Malaysia (UKM), Malaysia. Bachelor (Hons.) and Diploma in Electrical Engineering (Communication) (2002), UiTM Shah Alam, Malaysia

Dr. D. Amaranatha Reddy

Ph.D.(Postdocteral Fellow,Pusan National University, South Korea), M.Sc., B.Sc. : Physics.

Dr. Dibya Prakash Rai

Post Doctoral Fellow (PDF), M.Sc.,B.Sc., Working as Assistant Professor in Department of Physics in Pachhuncga University College, Mizoram, India.

Dr. Pankaj Kumar Pal

Ph.D R/S, ECE Deptt., IIT-Roorkee.

Dr. P. Thangam

BE(Computer Hardware & Software), ME(CSE), PhD in Information & Communication Engineering, currently serving as Associate Professor in the Department of Computer Science and Engineering of Coimbatore Institute of Engineering and Technology.

Dr. Pradeep K. Sharma

PhD., M.Phil, M.Sc, B.Sc, in Physics, MBA in System Management, Presently working as Provost and Associate Professor & Head of Department for Physics in University of Engineering & Management, Jaipur.

Dr. R. Devi Priya

Ph.D (CSE),Anna University Chennai in 2013, M.E, B.E (CSE) from Kongu Engineering College, currently working in the Department of Computer Science and Engineering in Kongu Engineering College, Tamil Nadu, India.

Dr. Sandeep

Post-doctoral fellow, Principal Investigator, Young Scientist Scheme Project (DST-SERB), Department of Physics, Mizoram University, Aizawl Mizoram, India- 796001.

Mr. Abilash

MTech in VLSI, BTech in Electronics & Telecommunication engineering through A.M.I.E.T.E from Central Electronics Engineering Research Institute (C.E.E.R.I) Pilani, Industrial Electronics from ATI-EPI Hyderabad, IEEE course in Mechatronics, CSHAM from Birla Institute Of Professional Studies.

Mr. Varun Shukla

M.Tech in ECE from RGPV (Awarded with silver Medal By President of India), Assistant Professor, Dept. of ECE, PSIT, Kanpur.

Mr. Shrikant Harle

Presently working as a Assistant Professor in Civil Engineering field of Prof. Ram Meghe College of Engineering and Management, Amravati. He was Senior Design Engineer (Larsen & Toubro Limited, India).

Table of Contents

Study of Non-Stationary Thermomechanical Processes in the Structure Elements of the Construction Taking into Accounting for the Local Surface Heat Exchanges

Dr. Sairanbek Akhmetov[1], Dr. Zhanna Iklasova[2]

[1]Department of technological machines and equipment, S. Seifullin Kazakh agrotechnical University, Astana– 010000, Kazakhstan

[2]Department of Fluid and Gas Mechanics, S. Utebayev Atyrau University of oil and gas, Atyrau – 060000, Kazakhstan

Abstract— *The aim of the work was to develop a methodology for taking into account the presence of local surface heat exchanges in rods of finite length, often taking place in studies of the non-stationary phenomenon of thermal conductivity. The proposed methodology was oriented to the subsequent creation of a computational algorithm and its implementation on a personal computer using the universal DELPHI programming tool. This allowed the authors to complete the initial stage of the research works, which will subsequently take into account the internal heat sources in the rods of finite length and constant cross-section in the study of non-stationary thermal conductivity, as well as to develop new methods, approaches and models associated with them.*

Keywords— finite length rod, internal heat sources, local surface heat transfer, non-stationary thermal conductivity, programming tools, thermomechanical processes.

I. INTRODUCTION

In mechanical engineering, in particular, in instrument engineering, plastic engineering, and also in other areas, physicotechnical processes often arise, where, any structural element in the form of a rod of finite length is suddenly exposed to thermomechanical loading [1]. Thermomechanical load can be in the form of local temperatures, heat fluxes or heat exchanges, where, in the case of their action on rods of finite length and constant cross-section, non-stationary thermal conductivity can occur in the system, as well as other non-stationary thermoelastic processes [2].

In practice, such phenomena are often encountered at the start of gas-generating, nuclear, hydrogen power plants, rocket and hydrogen engines, as well as internal combustion engines. In transient, unsteady heat conduction processes in the load-bearing elements of these power plants or engines, a complex non-stationary thermally stressed deformed state arises. Herewith, in order to study these processes, many load-bearing elements of the above-mentioned structures can be taken as rods of finite length with a constant cross-section along the entire length. For an adequate description of a non-stationary heat conduction process arising in the rod under the action of dissimilar types of heat sources, taking into account the presence of local thermal insulation, it is necessary to use the classical laws of energy conservation [3], because, the application of energy conservation laws describing such complex non-stationary processes of thermal conductivity in rods of finite length that are exposed to dissimilar kinds of heat sources allows us to take into account natural boundary conditions. As a result, the results obtained will have high accuracy [4]. This, in turn, will contribute to a correct evaluation of the thermally steady-state behavior of the bearing elements [5]. In connection with this, therefore, the development of special effective methods for investigating the non-stationary processes of thermal conductivity of load-bearing elements in the form of rods of finite length and constant cross-section is an actual problem of the applied non-stationary theory of thermoelasticity. At the same time, the development of a complex of applied DELPHI programs that allow studying the classes of non-stationary heat conduction processes for the above systems under the influence of dissimilar types of heat sources, taking into account the presence of local thermal insulation, is of independent scientific interest.

II. THE DEVELOPMENT OF THE METHODOLOGY RESULTS AND DISCUSSION

2.1 Algorithm for the construction of local approximating splines of a function

Based on the known technique [6] consider a horizontal discrete element of a rod of length l [cm] and a constant cross-sectional area F [cm^2]. Coefficient of thermal conductivity of the rod material is k_x [W/cm^{o}C]. We direct the horizontal axis

X, which coincides with the axis of the discrete element of the rod. The calculated scheme of the discrete element of the rod under consideration is shown in Fig. 1.

Suppose that the law of temperature distribution along the length of the discrete element is *T=T(x)*, where *x* is unknown. In the local coordinate system (*T,x*), $0 \leq x \leq l$we introduce the following notation $T(x=0)=T_i$; $T\left(x=\frac{l}{2}\right)=T_j$; $T(x=$ $l=Tk$. These notations are shown in Fig. 2.

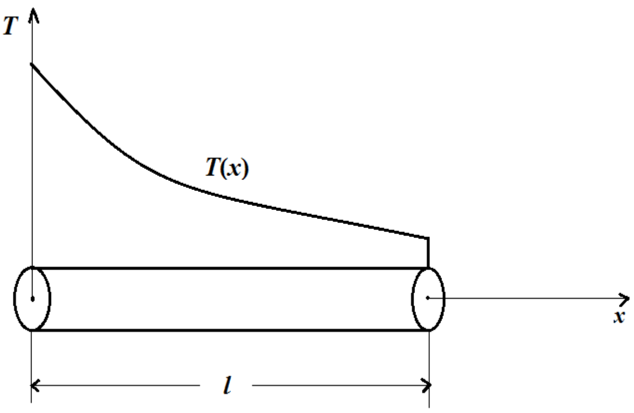

FIGURE 1: Calculation Scheme of the Discrete Element of the Rod

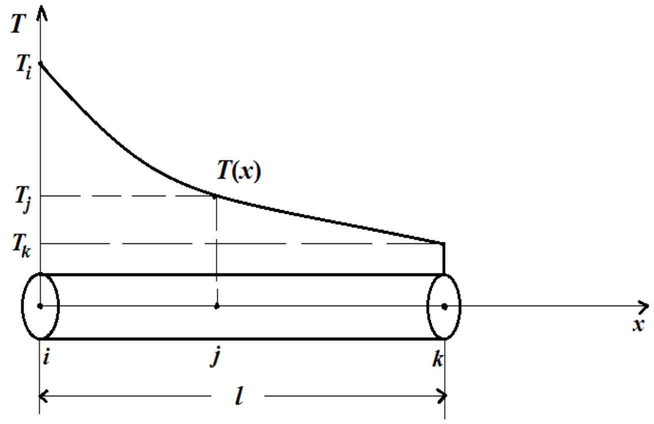

FIGURE 2: The Design Scheme in the Notation of the Local Coordinate System (T,X)

We denote the node with coordinate *x*=0by*i*, *x*=*l*/2 by *j* and *x*=*l* by *k*. n the notation adopted, we can construct the following approximating quadratic function

$$T(x)=ax^2+bx+c, 0 \leq x \leq l \tag{1}$$

a, *b*, *c* – are some constant values that are not yet known. In addition, also using the adopted notation, we have

$$\left.\begin{array}{c} T(x=0)=a\cdot 0+b\cdot 0+c=T_i \\ T\left(x=\frac{l}{2}\right)=a\cdot(\frac{l}{2})^2+b\cdot\frac{l}{2}+c=T_j \\ T(x=l)=a\cdot l^2+b\cdot l+c=T_k \end{array}\right\} \tag{2}$$

Solving this system, we determine the values of the constants *a*, *b*, *c*.

$$c=T_i, \tag{3}$$

$$\left.\begin{array}{c} \frac{al^2}{4}+\frac{bl}{2}=T_j-T_i \\ al^2+bl=T_k-T_i \end{array}\right\} \tag{4}$$

From the last two equations we have$al^2=T_k-T_i-bl$; $al^2+2bl=4T_j-4T_i$;or$T_k-T_i-bl+2bl=4T_j-4T_i$;or$bl=4T_j-4T_i-T_k+T_i$. Hence we define the value of *b*

$$b=\frac{4T_j-3T_i-T_k}{l} \tag{5}$$

Substituting (5) into the second equation of system (4), we obtain

$al^2=T_k-T_i+3T_i+T_k-4T_j=2T_k-4T_j+2T_i$;

From this we find the value *a*

$$a=\frac{2T_k-4T_i+2T_i}{l^2} \tag{6}$$

Further, substituting the found values of the constant parameters *a*, *b* and *c* in (1) we obtain

$$T(x)=\frac{2T_k-4T_i+2T_i}{l^2}x^2+\frac{4T_j-3T_i-T_k}{l}x+T_i, 0 \leq x \leq l \tag{7}$$

We simplify equation (7) according to the scheme$(\ldots)T_i + (\ldots)T_j + (\ldots)T_k$

$$T(x) = \left(\frac{2x^2}{l^2} - \frac{3x}{l} + 1\right)T_i + \left(\frac{4x}{l} - \frac{4x^2}{l^2}\right)T_j + \left(\frac{2x^2}{l^2} - \frac{x}{l}\right)T_k =$$

$$= \left(\frac{2x^2 - 3lx + l^2}{l^2}\right)T_i + \left(\frac{4lx - 4x^2}{l^2}\right)T_j + \left(\frac{2x^2 - lx}{l^2}\right)T_k, 0 \le x \le l \quad (8)$$

Here we introduce the following notation

$$N_i(x) = \frac{2x^2 - 3lx + l^2}{l^2};\ N_j(x) = \frac{4lx - 4x^2}{l^2};\ N_k(x) = \frac{2x^2 - lx}{l^2}, \quad (9)$$

Then (8) can be rewritten in the following form

$$T(x) = N_i(x) \cdot T_i + N_j(x) \cdot T_j + N_k(x) \cdot T_k, 0 \le x \le l \quad (10)$$

It should be noted that the values of the node temperatures$T_i, T_j, T_k$are still unknown; the functions$N_i(x), N_j(x), N_k(x)$are approximate quadratic spline functions. Now we study their properties

$$\left.\begin{array}{c} N_i(x=0) = 1;\ N_j(x=0) = 0;\ N_k(x=0) = 0 \\ N_i\left(x = \frac{l}{2}\right) = 0;\ N_j\left(x = \frac{l}{2}\right) = 1;\ N_k\left(x = \frac{l}{2}\right) = 0 \\ N_i(x=l) = 0;\ N_j(x=l) = 0;\ N_k(x=l) = 1 \end{array}\right\} \quad (11)$$

From (10) it is also possible to determine the expression for the temperature gradient within the length of the discrete element under consideration.

$$\frac{\partial T}{\partial x} = \frac{\partial N_i(x)}{\partial x} \cdot T_i + \frac{\partial N_j(x)}{\partial x} \cdot T_j + \frac{\partial N_k(x)}{\partial x} \cdot T_k = \frac{4x - 3l}{l^2} \cdot T_i + \frac{4l - 8x}{l^2} \cdot T_j + \frac{4x - l}{l^2} \cdot T_k, 0 \le x \le l \quad (12)$$

In addition, from (9) it can also be determined that

$$N_i(x) + N_j(x) + N_k(x) = \frac{2x^2 - 3lx + l^2 + 4lx - 4x^2 + 2x^2 - lx}{l^2} = 1 \quad (13)$$

2.2 Development of methods for accounting the presence of local surface heat transfer

Now consider one discrete element, through the lateral surface of which there is a heat exchange with its surrounding medium. In addition, through the cross-sectional area of the ends of the discrete element of the rod, heat exchange with the surrounding medium also takes place. To begin with, consider the case where the heat transfer coefficient is the same everywhere $h\left[\frac{W}{cm^2 \cdot {}^\circ C}\right]$, the ambient temperature is $T_{amb}[{}^\circ C]$. It is required to construct a resolving system of ordinary differential equations, taking into account the simultaneous presence of local surface heat exchanges. The calculation scheme for the problem under consideration is shown in Fig. 3.

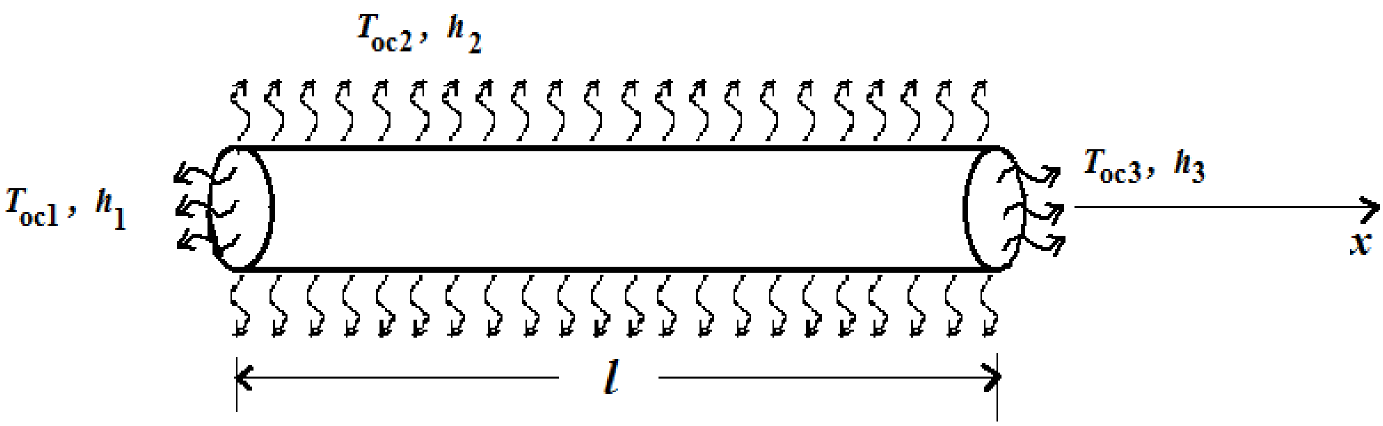

$$T_{amb\,1} = T_{amb\,2} = T_{amb\,3} = T_{amb}$$
$$h_1 = h_2 = h_3 = h$$

FIGURE 3: The Design Scheme of the Problem with Surface Heat Transfer

For the discrete element of the rod under consideration, taking into account the presence of local heat exchanges, we write the expression for the functional of the total thermal energy

$$\Pi = \int_V \frac{k_x}{2}\left(\frac{\partial T}{\partial x}\right)^2 dV + \int_V \lambda \frac{\partial T}{\partial t} T dV + \int_{S(x=0)} \frac{h}{2}(T - T_{oc})^2 dS + \int_{S_{ls}} \frac{h}{2}(T - T_{oc})^2 dS + \int_{S(x=l)} \frac{h}{2}(T - T_{oc})^2 dS \quad (14)$$

Where V is the volume of the discrete element of the rod; $S(x=0)$ is the cross-sectional area of the left end of the discrete element; $S_{ls}$is the area of the lateral surface of the discrete element of the rod; $S(x=0)$ is the cross-sectional area of the right end of the discrete element; $k_x\left[\frac{W}{°C \cdot cm}\right]$is the coefficient of thermal conductivity of the material of the rod, and λ is the heat capacity of the material of the rod, whose dimension is $\lambda\left[\frac{W \cdot sec}{cm^3 \cdot °C}\right]$.

In equation (14), the first term $\Pi_1 = \int_V \frac{k_x}{2}\left(\frac{\partial T}{\partial x}\right)^2 dV$ – physically means the amount of annulled heat quantity in the volume of the discrete element of the rod; the second term $\Pi_2 = \int_V \lambda \frac{\partial T}{\partial t} T dV$ is the change in the amount of heat per unit time; the other three terms mean the amount of heat that arises from convective heat transfer. Here, it should also be noted that the dimension of Π is $\Pi[W \cdot °C]$- i.e. the value of the heat work performed. In equation (14), the first term - physically means the amount of annulled heat quantity in the volume of the discrete element of the rod; The second term is the change in the amount of heat per unit time; The other three terms mean the amount of heat that arises from convective heat transfer. Here, it should also be noted that the dimension of P is P [W · °C] - i.e. The value of the heat work performed. Now let`s proceed to integrate all the terms of expression (14). Consider the first term of this functional

$\Pi_1 = \int_V \frac{k_x}{2}\left(\frac{\partial T}{\partial x}\right)^2 dV = F\int_0^l \frac{k_x}{2}\left(\frac{\partial T}{\partial x}\right)^2 dx,$ Substituting here the expression (12) we have

$$\begin{aligned}
\Pi_1 &= \frac{Fk_x}{2}\int_0^l \left[\frac{\partial N_i(x)}{\partial x}T_i + \frac{\partial N_j(x)}{\partial x}T_j + \frac{\partial N_k(x)}{\partial x}T_k\right]^2 dx = \\
&= \frac{Fk_x}{2l^4}\int_0^l \left[(4x-3l)T_i + (4l-8x)T_j + (4x-l)T_k\right]^2 dx = \\
&= \frac{Fk_x}{6l}\left(7T_i^2 - 16T_iT_j + 2T_iT_k - 16T_jT_k + 16T_j^2 + 7T_k^2\right),
\end{aligned} \quad (15)$$

Here the sum of the coefficients will be zero (7-16+2-16+16+7)=0.

Further we integrate the second integral of the functional (14)

$$\begin{aligned}
\Pi_2 &= \int_V \lambda \frac{\partial T}{\partial t} T dV = F\lambda \int_0^l \frac{\partial T}{\partial t} \cdot T dx = \\
&= F\lambda \int_0^l \left[N_i(x)\frac{\partial T_i}{\partial t} + N_j(x)\frac{\partial T_j}{\partial t} + N_k(x)\frac{\partial T_k}{\partial t}\right] \cdot \left[N_i(x)\cdot T_i + N_j(x)\cdot T_j + N_k(x)\cdot T_k\right] dx = \\
&= F\lambda \int_0^l \left[N_i^2(x)\cdot T_i \cdot \frac{\partial T_i}{\partial t} + N_i(x)\cdot N_j(x)\cdot T_j \cdot \frac{\partial T_i}{\partial t} + N_i(x)\cdot N_k(x)\cdot T_k \cdot \frac{\partial T_i}{\partial t} + \right. \\
&= N_i(x)\cdot N_j(x)\cdot T_i \cdot \frac{\partial T_j}{\partial t} + N_j^2(x)\cdot T_j \cdot \frac{\partial T_j}{\partial t} + N_j(x)\cdot N_k(x)\cdot T_k \cdot \frac{\partial T_j}{\partial t} + \\
&\left. + N_i(x)\cdot N_k(x)\cdot T_i \cdot \frac{\partial T_k}{\partial t} + N_j(x)\cdot N_k(x)\cdot T_j \cdot \frac{\partial T_k}{\partial t} + N_k^2(x)\cdot T_k \cdot \frac{\partial T_k}{\partial t}\right] dx
\end{aligned} \quad (16)$$

In this equation, integrating each integral (of nine) separately and substituting them into (16), we obtain the integrated form ofΠ_2;

$$\Pi_2 = F\lambda l\left[\frac{1}{15}T_i\frac{\partial T_i}{\partial t} + \frac{1}{15}T_j\frac{\partial T_i}{\partial t} - \frac{1}{30}T_k\frac{\partial T_i}{\partial t} + \frac{1}{15}T_i\frac{\partial T_j}{\partial t} + \right.$$
$$\left. + \frac{8}{15}T_j\frac{\partial T_j}{\partial t} + \frac{1}{15}T_k\frac{\partial T_j}{\partial t} - \frac{1}{30}T_i\frac{\partial T_k}{\partial t} + \frac{1}{15}T_j\frac{\partial T_k}{\partial t} + \frac{2}{15}T_k\frac{\partial T_k}{\partial t}\right] \quad (17)$$

Now, in the expression (14) we calculate the third integral

$$\Pi_3 = \int_{S(x=0)} \frac{h}{2}(T - T_{oc})^2 dS = \frac{Fh}{2}(T_i - T_{oc})^2 = \frac{Fh}{2}\left(T_i^2 - 2T_iT_{oc} + T_{oc}^{\ 2}\right) \quad (18)$$

Similarly, we can calculate the fifth integral in expression (14)

$$\Pi_5 = \int_{S(x=l)} \frac{h}{2}(T - T_{oc})^2 dS = \frac{Fh}{2}(T_k - T_{oc})^2 = \frac{Fh}{2}\left(T_k^{\ 2} - 2T_kT_{oc} + T_{oc}^{\ 2}\right) \quad (19)$$

In the expressions (18) ... (19) the sum of the coefficients will be equal to zero (1–2+1)=0.

The computation of the fourth integral in expression (14) will not be easy

$$\Pi_4 = \int_{S_{n\delta n}} \frac{h}{2}(T - T_{oc})^2 dS = \frac{Ph}{2}\int_0^l (T - T_{oc})^2 dx = \frac{Ph}{2}\int_0^l \left[(N_i(x)\cdot T_i + N_j(x)\cdot T_j + N_k(x)\cdot T_k) - T_{oc}\right]^2 dx =$$
$$= \frac{Ph}{2}\int_0^l \left[(N_i(x)\cdot T_i + N_j(x)\cdot T_j + N_k(x)\cdot T_k) - T_{oc}\right]\left[(N_i(x)\cdot T_i + N_j(x)\cdot T_j + N_k(x)\cdot T_k) - T_{oc}\right] dx = \quad (20)$$
$$= \frac{Ph}{2}\int_0^l \left[N_i^{\ 2}(x)\cdot T_i^2 + 2N_i(x)\cdot N_j(x)\cdot T_i\cdot T_j + 2N_i(x)\cdot N_k(x)\cdot T_i\cdot T_k - 2N_i(x)\cdot T_i\cdot T_{oc} + \right.$$
$$\left. + N_j^{\ 2}(x)\cdot T_j^{\ 2} + 2N_j(x)\cdot N_k(x)\cdot T_j\cdot T_k - 2N_j(x)\cdot T_j\cdot T_{oc} + N_k^{\ 2}(x)\cdot T_k^{\ 2} - 2N_k(x)\cdot T_k\cdot T_{oc} + T_{oc}^{\ 2}\right] dx$$

Where P is the perimeter of the cross-section of the discrete element of the rod. Now calculate each integral in expression (20)

$$K_1 = \int_0^l N_i^{\ 2}(x)\cdot T_i^{\ 2} dx = \frac{2l}{15}T_i^{\ 2} \quad (21)$$

$$K_2 = \int_0^l 2N_i(x)\cdot N_j(x)\cdot T_i\cdot T_j dx = \frac{2l}{15}T_iT_j \quad (22)$$

$$K_3 = \int_0^l 2N_i(x)\cdot N_k(x)\cdot T_i\cdot T_k dx = -\frac{l}{15}T_iT_k \quad (23)$$

$$K_4 = \int_0^l -2N_i(x)\cdot T_i\cdot T_{oc} dx = -\frac{2}{l^2}\int_0^l (2x^2 - 3lx + l^2)T_iT_{oc} dx =$$
$$= -\frac{2}{l^2}\left(\frac{2x^3}{3} - \frac{3lx^2}{2} + lx\right)\Big|_0^l T_iT_{oc} = -\frac{2l^3}{l^2}\left(\frac{4-9+6}{6}\right)T_iT_{oc} = -\frac{l}{3}T_iT_{oc} \quad (24)$$

$$K_5 = \int_0^l N_j^{\ 2}(x)\cdot T_j^{\ 2} dx = \frac{8l}{15}T_j^{\ 2} \quad (25)$$

$$K_6 = \int_0^l 2N_j(x)\cdot N_k(x)\cdot T_j\cdot T_k dx = \frac{2l}{15}T_jT_k \quad (26)$$

$$K_7 = \int_0^l (-2N_j(x)\cdot T_j \cdot T_{oc})dx = -\frac{2}{l^2}\int_0^l (4lx - 4x^2)T_j T_{oc}dx =$$
$$= -\frac{2}{l^2}(2lx^2 - \frac{4x^3}{3})\Big|_0^l T_j T_{oc} = -\frac{2l^3}{l^2}(\frac{6-4}{3})T_j T_{oc} = -\frac{4l}{3}T_j T_{oc} \tag{27}$$

$$K_8 = \int_0^l N_k{}^2(x)\cdot T_k{}^2 dx = \frac{1}{l^4}\int_0^l (2x^2 - lx)T_k{}^2 dx = \frac{1}{l^4}\int_0^l (4x^4 - 4lx^3 + l^2x^2)T_k{}^2 dx =$$
$$= \frac{1}{l^4}(\frac{4x^5}{5} - lx^4 + \frac{l^2x^3}{3})\Big|_0^l T_k{}^2 = \frac{l}{15}(12-15+5)T_k{}^2 = \frac{2l}{15}T_k{}^2 \tag{28}$$

$$K_9 = \int_0^l (-2N_k(x)\cdot T_k \cdot T_{oc})dx = -\frac{2}{l^2}\int_0^l (2x^2 - lx)T_k T_{oc}dx =$$
$$= -\frac{2}{l^2}(\frac{2x^3}{3} - \frac{lx^2}{2})\Big|_0^l T_k T_{oc} = -\frac{2l^3}{l^2}(\frac{4-3}{6})T_k T_{oc} = -\frac{l}{3}T_k T_{oc} \tag{29}$$

$$K_{10} = \int_0^l T_{oc}^2 dx = T_{oc}^2 \cdot x\Big|_0^l = lT_{oc}^2 \tag{30}$$

Now substituting (21) ... (30) into (20) we obtain the integrated form Π_4

$$\Pi_4 = \frac{Phl}{2}\left[\frac{2}{15}T_i^2 + \frac{2}{15}T_iT_j - \frac{1}{15}T_iT_k - \frac{1}{3}T_iT_{oc} + \frac{8}{15}T_j{}^2 + \frac{2}{15}T_jT_k - \frac{4}{3}T_jT_{oc} + \frac{2}{15}T_k{}^2 - \frac{1}{3}T_kT_{oc} + T_{oc}{}^2\right] \tag{31}$$

It should be noted here that the sum of the coefficients before the temperatures will be zero

$$\frac{2}{15} + \frac{2}{15} - \frac{1}{15} - \frac{1}{3} + \frac{8}{15} + \frac{2}{15} - \frac{4}{3} + \frac{2}{15} - \frac{1}{3} + 1 = 0$$

Substituting (15), (17) ... (19) and (31) into (14), we find the integrated form of the total thermal energy functional:

$$\begin{aligned}\Pi &= \frac{Fk_x}{6l}\left(7T_i^2 - 16T_iT_j + 2T_iT_k - 16T_jT_k + 16T_j{}^2 + 7T_k{}^2\right) + \\ &+ F\lambda l\left[\frac{1}{15}T_i\frac{\partial T_i}{\partial t} + \frac{1}{15}T_j\frac{\partial T_i}{\partial t} - \frac{1}{30}T_k\frac{\partial T_i}{\partial t} + \frac{1}{15}T_i\frac{\partial T_j}{\partial t} + \right. \\ &+ \left.\frac{8}{15}T_j\frac{\partial T_j}{\partial t} + \frac{1}{15}T_k\frac{\partial T_j}{\partial t} - \frac{1}{30}T_i\frac{\partial T_k}{\partial t} + \frac{1}{15}T_j\frac{\partial T_k}{\partial t} + \frac{2}{15}T_k\frac{\partial T_k}{\partial t}\right] + \\ &+ \frac{Fh}{2}\left(T_i^2 - 2T_iT_{oc} + T_{oc}{}^2\right) + \frac{Fh}{2}\left(T_k{}^2 - 2T_kT_{oc} + T_{oc}{}^2\right) + \\ &+ \frac{Phl}{2}\left[\frac{2}{15}T_i^2 + \frac{2}{15}T_iT_j - \frac{1}{15}T_iT_k - \frac{1}{3}T_iT_{oc} + \frac{8}{15}T_j{}^2 + \frac{2}{15}T_jT_k - \frac{4}{3}T_jT_{oc} + \frac{2}{15}T_k{}^2 - \frac{1}{3}T_kT_{oc} + T_{oc}{}^2\right]\end{aligned} \tag{32}$$

Further, minimizing the functional Π with respect to the node values $T_i, T_j\, and T_k$ we obtain a resolving system of first-order ordinary differential equations with the corresponding initial conditions and taking into account existing local heat exchanges.

$$\frac{\partial\Pi}{\partial T_i} = 0; \rightarrow \frac{Fk_x}{6l}\left(14T_i - 16T_j + 2T_k\right) + F\lambda l\left(\frac{1}{15}\frac{\partial T_i}{\partial t} + \frac{1}{15}\frac{\partial T_j}{\partial t} - \frac{1}{30}\frac{\partial T_k}{\partial t}\right) +$$
$$+\frac{Fh}{2}(2T_i - 2T_{oc}) + \frac{Phl}{2}\left(\frac{4}{15}T_i + \frac{2}{15}T_j - \frac{1}{15}T_k - \frac{1}{3}T_{oc}\right) = 0;$$

$$\frac{\partial \Pi}{\partial T_j} = 0; \rightarrow \frac{Fk_x}{6l}\left(-16T_i + 32T_j - 16T_k\right) + F\lambda l\left(\frac{1}{15}\frac{\partial T_i}{\partial t} + \frac{8}{15}\frac{\partial T_j}{\partial t} + \frac{1}{15}\frac{\partial T_k}{\partial t}\right) +$$

$$+\frac{Phl}{2}\left(\frac{2}{15}T_i + \frac{16}{15}T_j + \frac{2}{15}T_k - \frac{4}{3}T_{oc}\right) = 0;$$

$$\frac{\partial \Pi}{\partial T_k} = 0; \rightarrow \frac{Fk_x}{6l}\left(2T_i - 16T_j + 14T_k\right) + F\lambda l\left(-\frac{1}{30}\frac{\partial T_i}{\partial t} + \frac{1}{15}\frac{\partial T_j}{\partial t} + \frac{2}{15}\frac{\partial T_k}{\partial t}\right) +$$

$$+\frac{Fh}{2}\left(2T_k - 2T_{oc}\right) + \frac{Phl}{2}\left(-\frac{1}{15}T_i + \frac{2}{15}T_j + \frac{4}{15}T_k - \frac{1}{3}T_{oc}\right) = 0.$$

Or, after simplification from the last system, we get:

$$\begin{cases} \frac{\partial T_i}{\partial t} + \frac{\partial T_j}{\partial t} - \frac{1}{2}\frac{\partial T_k}{\partial t} + \left(\frac{35k_x}{\lambda l^2} + \frac{15h}{\lambda l} + \frac{2Ph}{F\lambda}\right)T_i + \left(\frac{Ph}{F\lambda} - \frac{40k_x}{\lambda l^2}\right)T_j + \left(\frac{5k_x}{\lambda l^2} + \frac{Ph}{2F\lambda}\right)T_k = \frac{15hT_{oc}}{\lambda l} + \frac{5PhT_{oc}}{2F\lambda} \\ \frac{\partial T_i}{\partial t} + 8\frac{\partial T_j}{\partial t} + \frac{\partial T_k}{\partial t} + \left(\frac{Ph}{F\lambda} - \frac{40k_x}{\lambda l^2}\right)T_i + \left(\frac{80k_x}{\lambda l^2} + \frac{8Ph}{F\lambda}\right)T_j + \left(\frac{Ph}{F\lambda} - \frac{80k_x}{\lambda l^2}\right)T_k = \frac{10PhT_{oc}}{F\lambda} \\ -\frac{1}{2}\frac{\partial T_i}{\partial t} + \frac{\partial T_j}{\partial t} + 2\frac{\partial T_k}{\partial t} + \left(\frac{5k_x}{\lambda l^2} - \frac{Ph}{2F\lambda}\right)T_i + \left(\frac{Ph}{F\lambda} - \frac{40k_x}{\lambda l^2}\right)T_j + \left(\frac{35k_x}{\lambda l^2} + \frac{15h}{\lambda l} + \frac{2Ph}{F\lambda}\right)T_k = \frac{5PhT_{oc}}{F\lambda} \end{cases} \quad (33)$$

Setting the initial conditions

$$T_i\big|_{t=0} = a_1;\ T_j\big|_{t=0} = a_2;\ T_k\big|_{t=0} = a_3$$

one can find a solution of the system (33).

The obtained results are oriented for the computational algorithm created by the authors, which was realized in a personal computer in the form of Delphi programs [7]. With the help of the Delphi-7 programming developed on the object-oriented programming language, we solved the non-stationary heat conduction problem for a rod of finite length under the influence of local heat transfer along the lateral surface [8].

III. CONCLUSION

Based on the energy conservation laws, a technique is developed that simultaneously takes into account the presence of local surface heat exchanges for the non-stationary heat conduction problem occurring in a rod of finite length and the constancy of its cross-sectional area. Applying the quadratic approximation function of the form from the energy conservation law by the method of minimizing it through the node temperature values, we obtain solving systems of first-order linear ordinary equations that take into account the natural boundary conditions. Due to this, the results obtained have a high degree of accuracy. The developed methodology and the corresponding computational algorithm allowed to realize calculations in a personal computer on the object-oriented Delphi-7 programming language, and thus to solve the non-stationary heat conduction problem for a rod of finite length under the influence of local heat exchange along the lateral surface.

REFERENCES

[1] O.A. Maugin, "The Thermomechanics of Nonlinear Irreversible Behaviors: An Introduction", Singapore: World Scientific, 1999, 375 p.

[2] D.Pantusoa, Klaus-Juergen Bathe, P.A.Bouzinov,"A finite element procedure for the analysis of thermo-mechanical solids in contact", Computers and Structures 75, 2000, Vol. No. 2, pp. 551- 573.

[3] T.Belytschko, У. Guo,W.Liu,S.Xiao,"A unified stability analysis of meshless particle methods", International Journal for Numerical Methods in Engineering, 2000, No. 48 (9), pp. 1359-1400.

[4] J. Deang,Q. Du, M.Gunzburger, "Modeling and computation of random thermal f1uctuations and material defects in the Ginzburg-Landau model for superconductivity", Journal of Computational Physics, 2002, Vol. 181, 2001, pp. 45-67.

[5] M.E.Gurtin, "An Introduction to Continuum Mechanics", New York: Academic Press, 1981, 830 p.

[6] B.A. Biswajit,"Material Point Method Formulation for Plasticity", Computational Physics, 2006, Vol. 51, pp. 1-25.

[7] Zh.Tashenova, N. Uzakkyzy, D. Omarkhanova, E. Nurlybaeva, A.Kudaykulov."Algorithm for calculation of parameters of the bearing elements of oil heating installation", IMPACT: International Journal of Computational Sciences and Information Technology, 2015, Vol. No. 1, Issue 1,pp. 13-19.

[8] Zh.Tashenova, E.Nurlybaeva, A. Kudaykulov, N.Tashatov, “Modeling of Thermo-Stressed State of Heat-Resistant Alloy Rod in the Presence of Temperature Constant Intensity”, Computer Sciences and Application, 2015. Vol. 2, No.4, pp. 157-160.

Dr. SairanbekAkhmetov is a Professor of the S. Seifullin Kazakh agrotechnical University, who made researches in mechanisms and machinery dynamics; moreover, he is the editor-in-chief and chairman of the editorial board of several Russian and Kazakh scientific journals, an acting member of the National Academy of the Republic of Kazakhstan and of the Russian Academy of Natural Sciences. He published more than 260 scientific papers, prepared 19 PhD in technical direction.

PhD ZhannaIklasova is a associate Professor of the S. UtebayevAtyrau University of oil and gas, he is a specialist in the field of machine dynamics in the oil and gas industry.

Contribution to the Determination of the Elasticity Modules of a Material (*Borassus Aethiopum*) based on an Experimental Method: Effort (Force)/Elongation or Moment/Degree ratio

Komlan LOLO[1], Ayarema AFIO[2], Sinko BANAKINAO[3], Kodjo ATTIPOU[4], Prof. Sonnou TIEM[5]

[1,2,4,5]Mechanical Research Team, Department of Mechanical Engineering, École Nationale Supérieure d'Ingénieurs (ENSI), University of Lome, 01 BP 1515 Lome 01, Lome, TOGO.

[3]Mechanical Research Team, Department of Civil Engineering, École Nationale Supérieure d'Ingénieurs (ENSI), University of Lome, 01 BP 1515 Lome 01, Lome, TOGO.

Abstract— *The mechanical characterization of a material involves the determination of longitudinal elastic modulus, the transverse modulus and the fish coefficient. To Obtaining these data is subject to experimentation. To obtain these data, there is need to experimentation. Several conditions contribute to the realization to the carrying out of the tests.To achieve this, there are methods which make it possible to better know the materials in general and especially the building materials by working on very small samples. Machinery, sample deposits and working conditions are obstacles to research. A civil engineering CBR press enabled us, during the three-point bending test, to determine the modulus of longitudinal elasticity by increasing the press force and elongation. Based on the example of bending, the transverse module is obtained by the torsion test based on the torsion moment and the torsion angle.*

The method is based on consideration of the Bending Effort/Elongation ratio or Moment/Torsion angle ratio. The experimental material is an object with its own morphology, the wandering wood. The difficulty of the work is related to the accuracy of all components of the sample.This method complements previous methods and puts into practice the indispensable dimensions of the strength of the materials.It shows the purpose pursued by an engineer in these experiments.

Keywords— Engineer, Characterizations, Essential quantities, Simple Technique, Rônier.

I. INTRODUCTION

One of the ways to know a material and its solicitation behavior is the characterization. It can be done in several fields: physics, mechanics, acoustics,... and in several ways. But for each domain, the characterization follows rules and principles: it is based on laws. It depends on the information sought. The main characterization techniques are mechanical tests, non-destructive tests and physico-chemical analyzes. In the case of mechanical and rheological characterization, machines or apparatus such as a mechanical phenomena analyzer, a rheometer, a bending machine are indicated for destructive or non-destructive tests based on the vibratory method in which the specimen is not destroyed.

Depending on the method of testing (destructive or not), methods such as the vibratory method, the ultrasonic method adopted on "Stress grading" are also used. Vibratory tests led to the determination of the longitudinal elastic modulus (MOE). Authors (Jehl et al, 2011, Viguier et al, 2015, JG van de Kuilen, 2002) have revealed the importance of the vibratory method. A similar method is the ultra sonic method of analyzing the speed of sound propagation in the sample. Another method based on the diffusion of X-rays. The aim is to measure the flux of ray that passes through the material over a period of time.These methods are performed on specified equipments or machines having sensors or detectors reading dimensional extensions. The principle must meet standards. In these standards, the experimental conditions**,** the number, the shape and the dimensions of the sample are to be respected.The characterization work must be carried out on the most suitable apparatus and machines [1]. The technique of the shapes of the materials must dictatethe shape of the samples. Experience data are to be considered. Unfortunately, these parameters differ according to the materials and objects to be manufactured. The damage during these characterization works is related to the testing machines and the popularity of samples. That is why we say the problem of the popularity of the samples remains.

Experimental material is limited. The probability of finding the same sample with the same characteristics is low. This is similar to archeology studies. It is very rare to be able to carry out physic-mechanical characterizations on old materials found in excavations or on works in restoration. However, the validation of results now a day's requires, from the statistical point of view, a considerable number of samples. The same samples are therefore rare to be identified because we cannot have the same morphology for samples taken from a tree or a portion of a tree. The elastic properties are characteristic of solid items, wood included. Elasticity means that the deformations are temporary. The body resumes its original dimensions when the force is removed [2]. When an elastic material exhibits at the same time a linear relationshipbetween the stress and the deformation, it is called linearly elastic. This is the case for wood [3] [4] [5].In our case, characterization of the material rônier wood, an analysis of the mechanical behavior is the work sought. But the literature gives little information about morphology [3] [6] and virtues. The sap is used as local wine, the fruit is edible and the leaves are used to make fans, baskets, mats [7] [8]. Know about the particular wood that is the rônier. The rônier is a building material of tropical Africa. It consists of fibers [9].

Due to its difficult work, it is abandoned. The rônier already has its structure and cannot undergo any formulation of the constituents. The material is made according to the morphology and the metallurgy. Difficulties are other techniques; there are no working tools, twig-shaped fibers act as nails. However, the mechanical, electrical and thermal values are unknown. With mechanization, his work can be possible and less tedious. The interest of this work is to provide a simple technique for obtaining data without sophisticated machines.

II. EXPERIMENT

2.1 Presentation of the material

Our article is focused on the rônier of the scientific name *Borassus Aethiopum*. The rônier belongs to the family of Borassoïdeae, of the palm category. The rônier is a slow-growing plant, up to 18 to 20 m tall. At this size, the plant can be between 40 and 50 years old. He is from tropical Sahelian Africa. The trunk has a greyish color and a cylindrical shape imbued at times. It is formed of fibers, surmounted by palms in spread tuft. These leaves are similar to large fans. The trunk of the rônier is considered as a false trunk so called stipe [3] [10] [11]. It is very hard on the bark but spongy in the heart of the plant. The life of the plant is influenced by the soil, climate and living conditions. The influences of man, the bush fire, the presence of man act on its growth. The rônier presents two subjects: male subject bearing fruit and a female subject carrying fruit. The male has male inflorescences of about 1 m 80.The female subject, flowering, bears flowers that will become fruit. The fruits have a pale yellow color and are edible [7]. The trunk remains the essential part of our study. It is rot-resistant and highly resistant to xylophages, mollusks and termites [10].

In our study, a female subject was used. It may be 30 years old. This treated subject lived in a humid climate environment.The trunk is large, 0.66 m in diameter. The trunk of the plant is felled. Slices are taken. Work is carried out on the slices to extract specimen samples. The size of the samples follows standard NF B 51 008. It is presented in figure 1. The dimensions of the specimens have a prismatic shape of square section of 20 ± 0.2 mm side and a length of 360 ± 2 mm [12].It is cut into the length of wood grain.

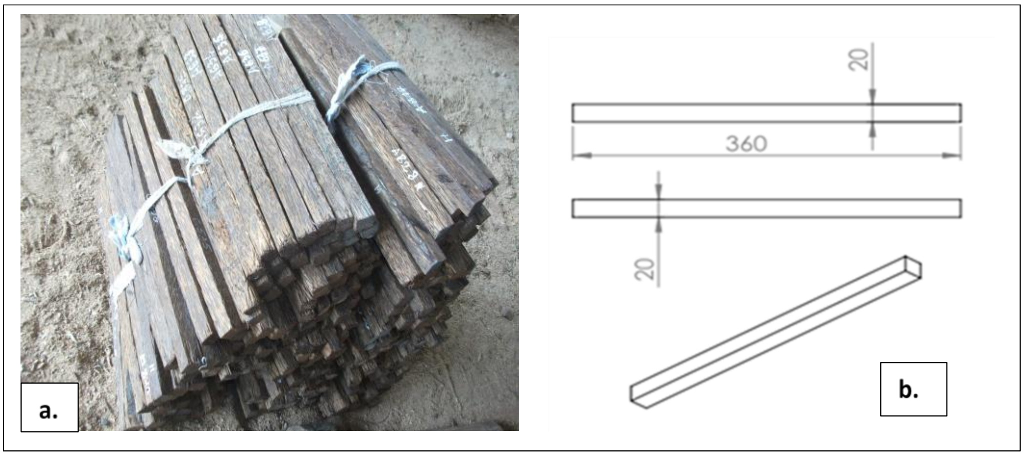

FIGURE 1: Shape of the samples
a. Samples put in piles b. Sizing of samples

Practical working machines are used. This is a CBR press, civil engineering and Tecquipment. The CBR press (fig. 2) is a compaction press. We attach to the press a device we have designed. The following figures show the CBR press and the Tecquipment (fig. 3).

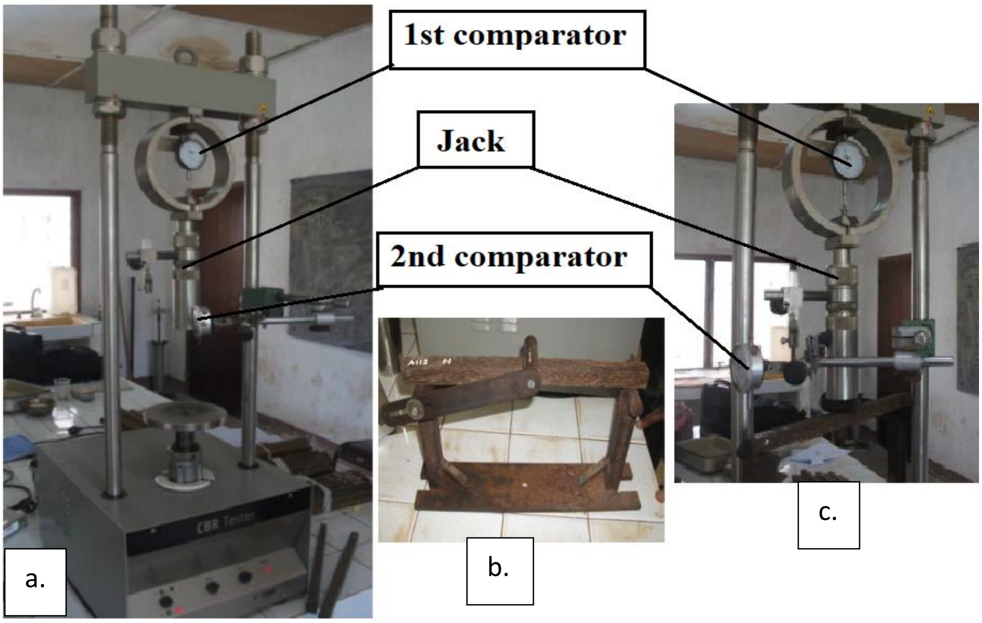

FIGURE 2: Experimental equipment
a. CBR civil engineering press; b. Testing device; c. Test Phase Device Sample

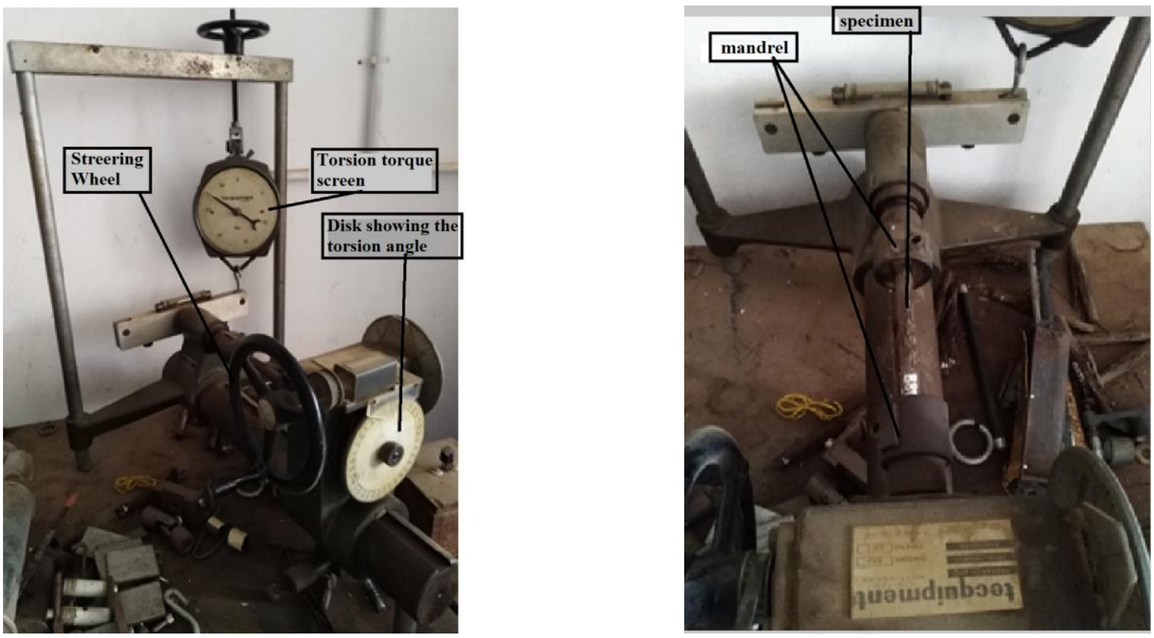

FIGURE 3: Torsion Device – Tecquipment

The CBR press is a press powered by electric current. It is equipped with a position switch that allows the machine to start. The approach speed is constant and is 1.27mm / min. The race is 120 mm. The pressing capacity is 50 kN. The load is applied by a motorized mechanical jack. The indicated speed is obtained by means of a reduction gearbox coupled to an electric motor of power 0.30 kW.

Tecquipment is an old test machine. It is a bench mounted machine. It is composed of two parts (I) and (II). Part (I) is intended for the torque reaction and a torquemeasurement system. This part has a dial capable of displaying torque. It also protects a torsion shaft supported by the bearings. The shaft carries a mandrel in which the test piece is mounted. Part (II) is the driving part where the mechanical force is applied to a crank. Through the reduction system, the rotation of the crank is transformed to some degree of deformation applied to the specimen. A decoder is used toread the number of rotation corresponding to the angle of torsion. It also carries a mandrel in which the specimen is mounted or tightened.

2.2 Description of the methodology

In this article, we present a technique developed for two different tests made of different devices. This is the bending test and the torsion test.

A civil CBR press is used in the bending test. The test carried out is the three-point bending. A civil engineering CBR press is used instead of a fatigue bench or a universal test machine. In performing the RDM tests, the engineer exploits some particular data that are integrated in the algorithm of the machine. These data enable longitudinal and transverse elongation to be obtained by means of sensors for tensile tests. Our technique is developed on a press on which we can obtain the pressing force and stroke of the box spring or apron. The sample is puton the test device that we designed. It rests on two cylindrical supports 320 mm apart. The press base (cylinder) goes down to press the test tube in the middle. The test begins when the comparator needle deviates. It ends when the test tube breaks.There is no deformation or elongation recorder on our press. Readings are made directly on the dial at selected time intervals. Every thirty (30) seconds, we read the position of the hands of the two comparators. From the experimental data (Force-Distortion distance), we plot the bending curve of the specimen in the elastic domain. The drawn curve follows the trend line whose equation is written next to it. The slope of this line is the ratio of the variation of these two sizes (Force-Distortion distance). However, as part of the characterization of the rônier, an experimental methodology was set up. It is the solution to our machine or work equipment problem. But if we do not have a modern universal machine with sensors, what should we do?

The values are recorded by the operator on the dial of the comparators. During the test, the value is read on the dial of a comparator. From an abacus accompanying the press allows to have the real value of the pressing force. A second comparator is placed 10 mm away from the outside and not toward the middle. It gives the value of the displacement. From these two data, a curve of the experiment is drawn. We deduce a ratio called stiffness K [13] in flexion (see relation 1).

$$K = \frac{\Delta F}{\Delta l} \tag{1}$$

ΔF: value of the force (N) and Δl: Distortion distance or elongation (mm).

The ratio K will be used in the search for longitudinal elastic modulus E (see relation 2).

$$E = \frac{1}{4b} \cdot \left(\frac{l}{h}\right)^3 . \boldsymbol{K} \tag{2}$$

l, b and h are the dimensions of the specimen or test piece (l: the length, b: the width and h: the height or thickness of the test piece).

For a torsion test, a similar method is used. It allows us to determine the shear module G (relations 3 and 4).

$$G = \frac{M_t}{\theta . I_0} \tag{3}$$

There for $\theta = \alpha / L$

L: length of the specimen.

From where

$$G = \frac{M_t}{\alpha} \cdot \frac{L}{I_0} \tag{4}$$

Here is a ratio of the torsion moment between torsion angle. We can write $\frac{M_t}{\alpha}$. By designating C this ratio, we can write C = f (α), that is to say that the moment is a function of the variation of the angle. The machine used is equipped with a crank of length **d**. When turning the crank, we vary the angle and read the force deployed **F**. The moment is the product (**F.d**). The angle of torsion is gradually changed. At each interval of 1 degree, the value of the corresponding force is read. An illustration is made of these obtained data. The relationship between moment and angle is given by equation 4.

For both methods, the linear part of the curves will be considered. It looks like a straight linewith a slope or guideline. The material is supposed to be elastic. With Excel spreadsheet, we find the equation of the line and therefore the slope. Said value makes it possible to find the longitudinal and transverse modules.

III. Results and Discussions

From the experimental data collected, different curves are drawn. The experiments are conducted until the sample is broken. Forcevalues correspond to elongations. A curve has a linear zone and a curvilinear zone. The linear zone reflects the elastic aspect of the material. The nonlinear or curvilinear zone is the illustration of the permanent deformation of the material. This deformation occurred as soon as the first constituents of the material were destroyed. In this article, we are interested in the linear part of the curve. The Excel spreadsheet gives us the corresponding line. The slope of the line is the ratio revealed by the engineer. From two examples, we present the technique that constitutes our contribution.

3.1 First evidence : Bending test

Forty-four (44) specimens were tested for the same type of trunk test. Here is the bending test result which is the illustrative curve of three samples tested. We record the effort in ordered and the arrow in abscissa. We obtain the complete curve illustrating the test from the beginning to the break. The curve thus obtained is similar to the curve having a linear part and a nonlinear part. The linear zone is the quasi linear zone that we will consider. The curve of the test is the illustration of all the information of the test. During the test, the breaking of the first fibers or the first deteriorations causes the change of the curve shape. So as soon as the curve is no longer linear, we have entered another phase. In this case, the material remains elastic up to 4.5 mm for a force corresponding to 900 N. Using our method, we draw the straightline and then calculate the longitudinal elastic modulus (MOE). The maximum deflection varies between 9 and 11.1 mm for an effort of between 922 and 1334 N.However, the determination of the MOE requires sophisticated machines and more indicated [1]. And if the sophisticated machine fails, it is necessary to consider techniques to prove the feasibility of the model. These curves are almost identical to those obtained on sophisticated machines. Despite the precautions taken, some distortions are observable on the curves. We attribute them to manufacturing errors related to cutting and handling conditions during the test. But the rônier is a material that does not break abruptly because of intertwined fibers. It is very elastic. One of these advantages is the absence of nodes.

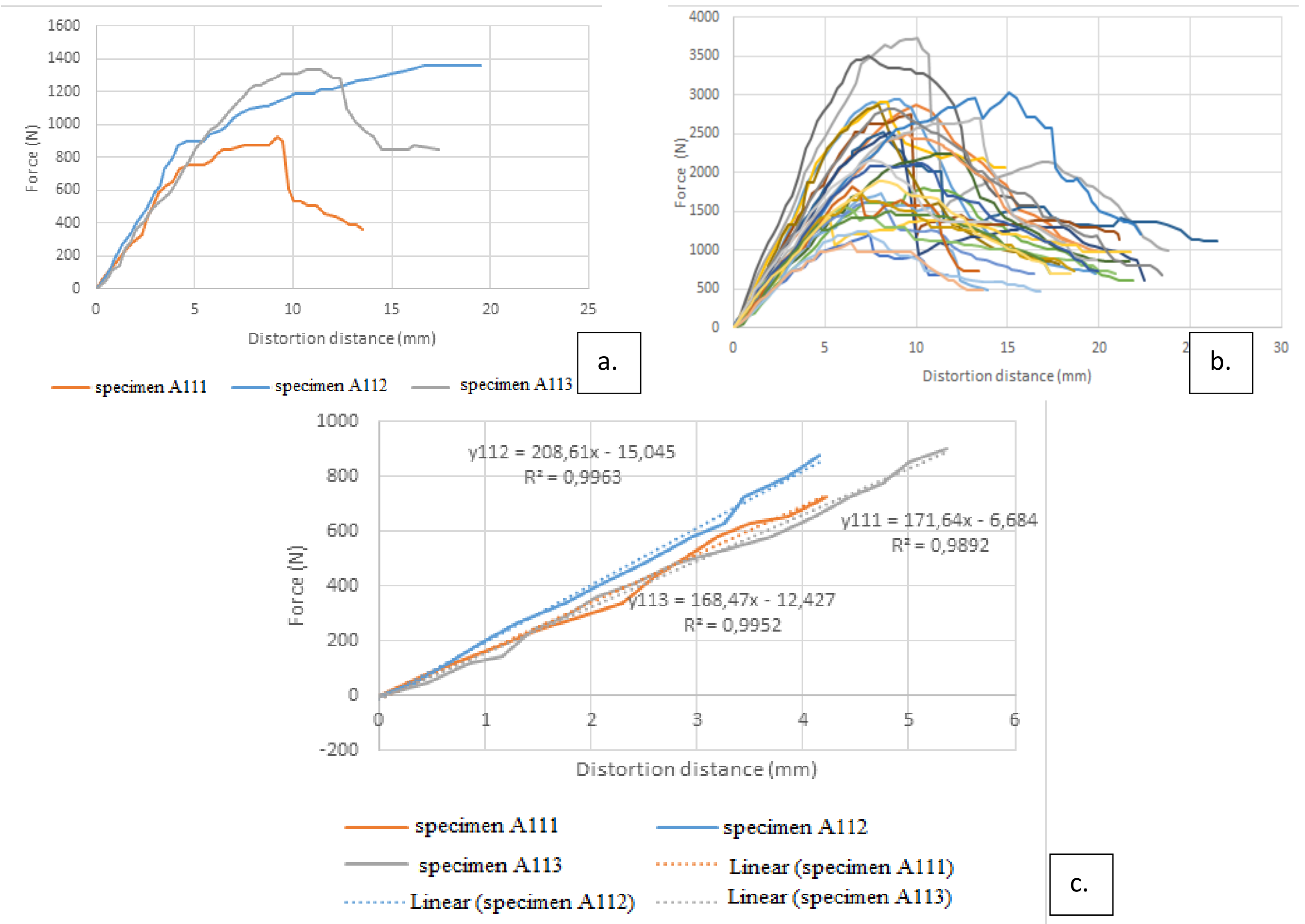

Figure 4: Presentation of the bending test result
a. Complete curve b. Curves grouping c. Linear portion of the curve

TABLE 1
RESULT OF EIGHT SLATS FROM THE TRUNK - MOE CALCULATION BASED ON K

N° slats	Code	Dimensions (mm)				Mass	ρ	Rigidity		MOE	Force
		e	h	e/h	L	m (g)	(g/cm^3)	K	R²	(N/mm^2)	(N)
L1	A111	20,7	21,0	0,986	360	143,55	0,92	177,64	0,98	10 808	922,3
	A112	23,2	20,2	1,149	360	165,85	0,98	208,61	1,00	12 724	1359,2
	A113	22,2	18,0	1,233	360	139,82	0,97	168,47	1,00	15 177	1334,9
	A114	20,3	23,0	1,133	360	158,16	0,94	207,48	0,97	9 798	1674,7
	A115	21	23,3	1,11	360	156,53	0,89	330,27	0,99	14 502	1626,2
	A116	19,5	22,5	1,154	360	144,12	0,91	272,06	0,99	14 287	1165
L2	A211	19,6	20	0,98	360	135,78	0,96	157,26	0,99	11 698	728,1
	A212	17,9	21,4	0,836	360	142,03	1,03	196,83	1,00	13 087	1043,6
	A213	20,8	19	0,913	360	140,4	0,99	180,05	1,00	14 720	946,6
	A214	20	19,29	0,965	360	136,25	0,98	192,73	1,00	15 659	1067,9
L3	A311	19,5	20,3	0,961	360	142,4	1,00	243,63	0,99	17 420	1019,4
	A312	20,6	20,6	1	360	150,28	0,98	180,14	0,99	11 668	1286,4
	A313	20,4	20,35	0,998	360	145	0,97	163,58	1,00	11 098	655,2
	A314	19,7	20	1,015	360	144,45	1,02	169,08	0,99	12 514	1165
L4	A411	22	21,6	1,019	360	148,57	0,87	166,84	0,99	8 777	995,1
	A412	22,8	20,7	1,101	360	154,77	0,91	203,78	0,99	11 753	1262,1
	A413	22,5	17,5	1,286	360	138,37	0,98	148,9	1,00	14 403	970,8
	A414	20	22	1,1	360	147,53	0,93	256,03	0,99	14 023	1189,3
	A415	20,5	21,6	1,054	360	147,56	0,93	204,35	0,98	11 537	1553,3
	A416	21	17,67	0,841	360	115,84	0,87	135,32	0,98	13 623	1140,7
L5	A511	18,9	17,4	1,086	360	116,1	0,98	109,34	0,99	12 809	1067,9
	A512	19,7	19,1	1,031	360	133,1	0,98	175,62	1,00	14 923	1432
	A513	19,9	20	0,995	360	141,6	0,99	127,07	1,00	9 310	752,4
	A514	18,6	20,3	1,091	360	138,59	1,02	168,74	1,00	12 649	558,2
	A515	17,8	19,8	1,112	360	130,13	1,03	143,32	0,98	12 099	315,5
	A516	20	20	1	360	140,42	0,98	155,21	0,99	11 315	703,8
L6	A611	20	20	1	360	122,65	0,85	162,16	1,00	11 821	1092,2
	A612	19,9	20	0,995	360	135,62	0,95	172,28	1,00	12 622	1213,5
	A613	20	19,1	1,047	360	129,48	0,94	171,43	1,00	14 348	1140,7
	A614	19,7	19,5	0,99	360	131,9	0,95	171,87	0,99	13 724	776,6
	A615	19,9	20	1,005	360	136,24	0,95	129,31	0,99	9 474	898
	A616	20	19,5	0,975	360	147,61	1,05	147,84	0,99	11 628	849,5
L7	A711	18	18,5	0,973	360	125,25	1,04	138,4	0,99	14 164	970,8
	A712	20	20	1	360	146,15	1,01	163,76	1,00	11 938	1456,3
	A713	18,4	20	0,92	360	138,93	1,05	155,28	1,00	12 304	1286,4
	A714	18,4	17,4	0,946	360	133,64	1,16	111,09	1,00	13 368	679
	A715	20,4	19,3	0,946	360	135,31	0,95	104,71	0,98	8 328	970,8
	A716	20	19,9	0,995	360	133,13	0,93	180,91	0,99	13 388	970,6
L8	A811	19,7	20,6	0,956	360	134,94	0,92	204,35	1,00	13 841	1699
	A812	20	20	1	360	144,26	1,00	174,34	0,99	12 709	1601,9
	A813	20	20	1	360	124,77	0,87	140,93	1,00	10 274	1577,6
	A814	20	19,4	0,97	360	140,63	1,01	142,17	1,00	11 356	266,9
	A815	20	20	1	360	149,62	1,04	238,77	0,99	17 406	1092,2
	A816	19,5	20	1,026	360	143,23	1,02	150,29	0,99	11 237	825,2
Average							**0,97**	**169,48**	**0,99**	**12 649**	**1 036**
Standard Deviation							**0,06**	**43,21**	**0,01**	**2 011**	**335**

Through the graph c. of figure 4, we see the pace of the various curves with deviations of the order of a thousand. The curves express the true or real behavior of the material. The dashed line represents the ideal curve. In this step, in order to validate our technique or method, we considered using the linear part of the experimental traced curve so as to correlate the obtained results with those obtained analytically. We use the slope value in the calculation of the longitudinal elastic modulus. The values of the lines are obtained with an accuracy of 0.021 for the coefficient of determination (R^2 = 0.9892). The error is therefore minimal. We note a similarity between the curve of the actual behavior and that of the ideal. Wecould have worked with a machine having elongation readers or sensors, we will not have largedifferencein measurements therefore in the layout. We start from this information mainly from the slope of the plotted curves to calculate the longitudinal elastic modulus (MOE). Density and MOE are classifying parameters of a material [1]. In the following table, we will see the MOE calculated on the basis of K (slope of the straight line) with the very significant coefficient of determination (R^2> 0.95). Table 1 shows the result of about forty-four samples tested at one level. This result is level 1(level very close to the bark). We have defined three levels. The trunk is divided into eight slats. The following table gives the wood (Rônier) density, the MOE and the force corresponding to a start of deformation.

At the end of the result, the MOE is 12649 daN/mm^2 with a standard deviation of 2010. This value is close to that of wood in general. The MOE of wood in general is between 10000 and 20000 daN/mm^2 according to the literature. The density is 0.97 g / cm^3 corresponding to that of wood in general. This density makes it possible to classify it among the heavy woods. The Rônier is a good quality wood.

3.2 Second evidence: Torsion test

This is the curve of a torsional sample. We record the moment in ordinate and the angle of torsion in abscissa. We see the complete curve and the linear area considered. The material remains elastic up to 8 degrees for a torsion moment equivalent to 337500 N mm.

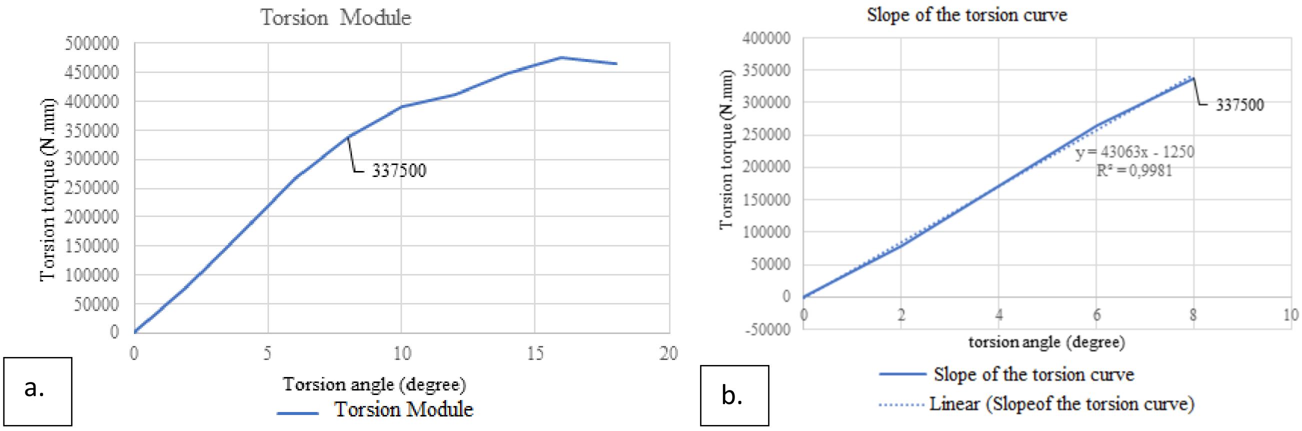

FIGURE 5: Presentation of the torsion test result
a. Complete curve b. Linear portion of the curve

We use the value of slopes in the calculation of the transverse modulus of elasticity. The value of the line is obtained with an accuracy of 0.002 (R^2 = 0.998). The error is therefore minimal.

This technique is based on the algorithm of the mechanical machines that record the data as if we are using a universal test machine. Thus through a fatigue machine or test bench, we performed almost the same bending curves. The errors are similar.

IV. CONCLUSION

Better knowledge of a material and its behavior in the face of the various demands require the deployment of an appropriate test machine and the important deposit to assess the quality of the result statistically. The absence of an adequate machine is solved by the development of a simple technique based on the ratio Stress / Elongation or Moment / Angle of torsion ratio. This experience constitutes the solution to the lack of machine. This technique will allow the learner to get to work. The combination of these two tests provides information about longitudinal and transverse modules with unexpected accuracy.

REFERENCES

[1] Y. Faydi, Classement pour la résistance mécanique du chêne par méthodes vibratoires et par mesure des orientations des fibres, Paris: HAL archives-ouvertes.fr, 2017.

[2] F. P. F. Kollmann et A. C. Wilfred, Principles of Wood Science and Technology, vol. 1, New York: Springer-Verlag, 1968.

[3] A. Ellouze, S. Ellouze et S. Medhioub, «Détermination des caractéristiques mécaniques du bois Tronc de Palmier,» *Innovation et valorisation en genie civil et matériaux de construction,* vol. 30, n° %1123, pp. 1 - 8, 2011.

[4] J. Campredon, «Contribution à l'étude des propriétés élastiques des bois,» Ann. Forest. T.V.- Fasc. 3, Paris, 1935.

[5] F. Meriem, «Propriétés mécaniques et physiques du bois,» Lorraine, 2015.

[6] P. Jaccard, «Évolution morphologique de la flore et structure anatomique du bois,» *Bulletin de la Société Vaudoise des Sciences Naturelles,* pp. 1 - 15, 2015.

[7] G. Yaméogo/Coulibaly, Les modes de gestion de Borassus aethiopum Mort. dans la Province du Koulpelogo, Bobo-Dioulasso (Burkina Faso): Université Polytechnique de Bobo-Dioulasso , 2007.

[8] R. Portères, «Le palmier (Borassus aethiopum mart) dans la province du Baoule (Côte d'Ivore),» *Journal d'agriculture tropicale et de botanique appliquée,* vol. 11, n° %112, pp. 499 - 514, Décembre 1964.

[9] K. Lolo et S. Tiem, «Singularité du Bois Borassus Aéthiopum par sa physiologie,» *Europian Scientific Journal,* vol. 13, n° %133, pp. 463 - 472, 30 Novembre 2017.

[10] A. Chevalier, «Le Borassus Aéthiopum de l'Afrique Occidentale et son utilisation.,» Revue scientifique, 1930.

[11] K. Lolo, S. Tiem et S. Banakinao, «Valorization of the Borassus Aethiopum wood behavior in tensile and bending,» *Research Journal of Engineering Sciences,* vol. 6, n° %111, pp. 20 - 29, 2017.

[12] B.-0. Norme Française NF, Bois - Caractéristiques Physiques et Mécaniques des Bois, p. 17, Paris: Association française de Normalisation.

[13] L. P. Giffard, «Le palmier rônier Borassus Aéthiopum Mart,» *Bois et Forêts des tropiques,* n° %1116, 1967.

[14] O. E. Onyekachi et K. O. Iwuozor, «Mechanical and Water Absorption Properties of Polymeric Compounds,» *American Journal of Mechanical and Materials Engineering* , vol. 3, n° %12, pp. 36 - 46, 2019.

[15] K. Korkmaz, S. Kocak, M. E. Gafy et E. Boztas, «Effects of Elastic Modulus on Behavior of Polymer Coated Fiber Modified Short Concrete Beams,» *American Journal of Construction and Building Materials,* vol. 3, n° %11, pp. 1-9, 2019.

[16] O. E. O. Kingsley Ogemdi Iwuozor, «Mechanical and Water Absorption Properties of Polymeric Compounds,» *American Journal of Mechanical and Materials Engineering,* vol. 3, n° %12, pp. 36-46, 2019.

[17] A. Prakasan et O. A. Mathews, «Experimental study on lateral behavior of step tapered piles in sand,» *International Journal of Engineering Research in Mechanical and Civil Engineering,* vol. 4, n° %17, pp. 33-37, 2019.

The computer modeling of the physical mechanism of the 2D convective transport of hydrocarbons from the mantle wedge to the Earth's surface: a comparison of the Newtonian and non-Newtonian rheology cases

Sergey Gavrilov[1*], Andrey Kharitonov[2]

[1]Schmidt Institute of Physics of the Earth of the Russian Academy of Sciences, IFZRAS, Moscow, Russia
[2]Pushkov Institute of Terrestrial Magnetism, Ionosphere and Radio Wave Propagation of the Russian Academy of Sciences, IZMIRAN, Moscow, Troitsk, Russia

Abstract— *For the non-Newtonian mantle rheology case the 2D thermal viscous dissipation-driven thermal convection in the mantle wedge above the Apulian lithospheric microplate subducting under the Euro-Asian plate is modeled numerically. The effects of the 410 km and 660 km phase transitions are taken into account. Within the framework of the model constructed the horizontal extent of the 2D heat flux anomaly observed in the rear of the Dinarides mountain belt corresponds to subduction velocity of ~10 mm per year which is close to that observed with the help of geodetic means. In the case of non-Newtonian rheology the upwelling convective flow transporting heat to the Earth's surface locates at the distance from the trench corresponding to the actually observed 2D heat flux anomaly, the velocity in the convective vortices being from ~10 mm per year to ~10 m per year for the water content in the mantle wedge from* 0.3×10^{-1} *to* 3×10^{-1} *weight percent respectively. The convection cell dimension is of the order of the horizontal scale of the heat flux anomaly observed in the Pannonia petroleum basin and Vardar zone. Upwelling mantle wedge convective flow is indicated to be able to provide the mantle wedge hydrocarbons transport to the Earth's surface for the mantle wedge mantle content over* 0.3×10^{-1} *weight percent.*

Keywords— Computer Modeling, Thermal Convection, Newtonian & Non-Newtonian Rheology Cases.

I. INTRODUCTION

According to [3], the subduction of the Apulian lithospheric microplate under the Dinarides, Pannonia basin and Vardar zone is sufficiently flat and during the last ~ 45 Ma occurred at the angle of ~ 25°, which remained unchanged during this time interval. The genesis of the Dinarides mountain belt (with the transversal horizontal extent of ~ 300 km) apparently is of the thrust and fold nature, associated with the former collision and subduction of the oceanic branches of the Neo-Tethis and Alpine-Tethis as the result of thrusting of the African plate under the Eastern and Western Europe during the last 55 – 35 Ma [3]. In [1] numerous papers are referred, containing contradictory estimates of the relative motions of the Apulian lithospheric microplate and Euro-Asian plates, made on the basis of seismic, geophysical and geodetic data. In fig. 3 in [Op. cit.] the velocity of subduction of the Apulian lithospheric microplate under the Euro-Asian one is seen to amount to ~5 – 8 $mm\times a^{-1}$ according to referred works, while in [1] this velocity is estimated to be of the order of ~ 5 $mm\times a^{-1}$ according to calculations based on geodetic observations. In [12] the Pannonia petroleum basin and Vardar zone are noted to be the zones of the Middle Miocene extension occurred ~ 14 – 11.6 Ma ago, which led to the lithosphere thinning, these zones being the back-arc basin characterized by the back-arc spreading. At that time the single mountain belt parallel to Apulian shore was split into Carpathians and Dinarides and the shallow Pannonian sea was formed, which existed approximately to 600 thousand years ago. Presently the Pannonian oil- and gas-bearing basin is situated in this region. Here the conditions are clarified under which the centre of the back-arc spreading initiates as the result of convective instability, driven by the dissipative heat release in the mantle wedge above the subducting Apulian lithospheric microplate.

According to [4, 8, 9] two types of dissipation-driven small-scale thermal convection in the mantle wedge are possible, viz. the 3D finger-like convective jets, raising to volcanic chain, and 2D transversal Karig vortices, aligned perpendicularly to subduction. These two types of convection are shown to be spatially separated due to the pressure and temperature dependence of mantle effective viscosity, the Karig vortices, if any of them formed, being located behind the volcanic arc [4]. There are contradictory judgments on the velocity of subduction of the Apulian lithospheric microplate under the Euro-Asian one, although the order of magnitude of the present-day subduction velocity (~ 10 $mm\times a^{-1}$) can apparently be regarded as established sufficiently reliably. The mountainous massif Dinarides locates parallel to the north-eastern shore of the Adriatic sea, and probably is of the thrust-and-fold nature. The 2D maximum of the heat flux anomaly of ~100 $mW\times m^{-2}$

observed in the rear of the Dinarides massif in the Pannonia basin and the Vardar zone [10] can be assumed to owe its origin to the convective heat supply from the mantle wedge. Numerical modeling of the 2D convection, occurring in the mantle wedge in the form of the Karig vortices and presumably transporting heat upwards, allows to judge about the mean water content in the mantle wedge and to assume the mantle hydrocarbons to be transported to the Earth's surface by the upwelling convective flows. Numerical convection models accounting for the pressure-, temperature- and stress-dependence of viscosity fit best to observational data in the case of non-Newtonian rheology at the mantle water content of ~ (0.3 – 3)□ 10^1 weight % for the velocity of subduction of ~ 10 mm×a^{-1} during the Middle Miocene. In [15] such rather a high water content (and even greater one, up to 3 weight %) can be observed in the mantle wedge in the mantle transition zone. The Middle Miocene subduction velocity of ~10 mm×a^{-1} during the formation of the Pannonia basin is of the order of the observed presently, or, can somewhat exceed it because of the gradual diminution of the velocity of convergence of African and Euro-Asian plates.

II. THE COMPUTER THERMO-MECHANICAL MODEL

Thermo-mechanical model of the mantle wedge between the base of the overlying Euro-Asian plate and the upper surface of the Apulian lithospheric microplate subducting under the Euro-Asian one with a velocity V at an angle β is obtained for the infinite Prandtl number fluid as a solution of non-dimensional 2D hydrodynamic equations in the Boussinesq approximation

$$(\partial^2_{zz}-\partial^2_{xx})\times\eta\times(\partial^2_{zz}-\partial^2_{xx})\times\psi+4\times\partial^2_{xz}\eta\times\partial^2_{xz}\psi=Ra\times T_x-Ra^{(410)}\times\Gamma_x^{(410)}-Ra^{(660)}\times\Gamma_x^{(660)} \quad (1)$$

$$\partial_t T=\Delta T-(\psi_z\times T_x)+(\psi_x\times T_z)+(Di/Ra)\times(\tau^2_{ik}/2\times\eta)+Q \quad (2)$$

For the stream-function ψ and temperature T. Here η is dynamic viscosity, ∂ and indices denote partial derivatives with respect to coordinates x (horizontal), z (vertical) and time t, Δ is the Laplace operator, $\Gamma^{(410)}$ and $\Gamma^{(660)}$ are volume ratios of the heavy phase at the 410 km and 660 km phase boundaries, the velocity components V_X and V_Z are expressed through ψ as

$$V_X=\psi_z,\ V_Z=-\psi_x \quad (3)$$

while non-dimensional Rayleigh number Ra, phase numbers $Ra^{(410)}$, $Ra^{(660)}$ and dissipative number Di are

$$\begin{gathered}Ra=[(a\times\rho\times g\times d^3\times T_1)/(\eta_C\times\chi)]=5.55\times10^8;\\ Ra^{(410)}=[(\delta\rho^{(410)}\times g\times d^3)/(\eta_C\times\chi)]=6.60\times10^8;\\ Ra^{(660)}=[(\delta\rho^{(660)}\times g\times d^3)/(\eta_C\times\chi)]=8.50\times10^8;\\ Di=[(a\times g\times d)/c_p]=0.165,\end{gathered} \quad (4)$$

where $\alpha=3\times10^{-5}$ K^{-1} is the thermal expansion coefficient, ρ = 3.3 g × cm^{-3} is the density, g is gravity acceleration, c_p = 1.2×10^3 J × kg^{-1}× K^{-1} is specific heat capacity at constant pressure, T_1 = 1950°K is the temperature at the base of mantle transition zone (MTZ) at depth 660 km regarded the lower boundary of the model domain, $Q=6.25\times10^{-4}$ mW× m^{-3} is the volumetric heat generation in the crust, τ_{ik} is the viscous stress tensor, d = 660 km is vertical dimension of the modeled domain, $\eta_s=10^{18}$ Pa×s is the viscosity scaling factor, χ = 1 mm^2 ×s^{-1} is thermal diffusivity, $\delta\rho^{(410)}=0.07\rho$ and $\delta\rho^{(660)}=0.09\rho$ are the density changes at the 410 km and 660 km phase boundaries respectively. In (1), (2) the scaling factors for time t, coordinates x and z, stresses τ_{ik} and the stream-function ψ are $(d^2\times\chi^{-1})$, d, $(\eta_s\times\chi\times d^{-2})$ and χ respectively. Assuming rheology be linear for the diffusion creep deformation mechanism dominating in the mantle at depths over ~ 200 km [2], we accept the temperature- and lithostatic pressure p dependent viscosity as [15]:

$$\eta=(\mu/2\times A)\times(h/b^*)^m\times\{\exp[(E^*+p\times V^*)/(R\times T)]\} \quad (5)$$

where for "wet" olivine $A=5.3\times10^{15}$ s^{-1}, m = 2.5, the grain size $h=10^{-1}$ – 10 mm, $b^*=5\times10^{-8}$ cm is the Burgers vector [14], E^* = 240 kJ×mol^{-1} is activation energy, $V^*=5\times10^3$ mm^3·mol^{-1} is activation volume, μ = 300 GPa is the shear modulus normalizing factor, R is the gas constant. At the constants chosen and the grain size h =1.6 mm, non-dimensional viscosity also denoted η is

$$\eta=5\times10^{-7}\times\exp\{[14.8+6.72\times(1-z)]/T\} \quad (6)$$

where T is non-dimensional temperature, non-dimensional z normalized by d is pointing upwards from the MTZ base and x is pointing against subduction along the MTZ base. The aspect ratio of the model domain is 1:2.25 thus the subduction angle being $\beta=24°$ if subduction is assumed to take place along the model domain diagonal. Non-dimensional subduction velocity

V = 10 mm×a^{-1} normalized by ($\chi \times d^{-1}$) equals $V = 0.208\times10^3$, i.e. non-dimensional velocity components of subducting Adriatic micro-plate are $V_X = -0.190\times10^3$ and $Vz = -0.085\times10^3$.

To check as to how the estimate of velocity of subduction of the Adriatic micro-plate is sensitive to the accepted linear rheological law here we make extra computations for the non-Newtonian rheology, in which case the viscosity formulae (5)–(6) are rewritten as:

$$\eta = (1 / 2 \times A \times C_w^{\ r} \times \tau^{n-1}) \times (h / b^*)^{\mathrm{m}} \times \{ \exp [(E^* + p\times V^*) / (R \times T)] \} \tag{7}$$

where according to [13] for "wet" olivine $n = 3$, $r = 1.2$, $m = 0$, $\tau = (\tau^2_{\iota\kappa})^{1/2}$, E^*= 480 kJ·mol^{-1}, V^* = 11×10^3 mm^3×mol^{-1}, A = 10^2 c^{-1}×(MPa)$^{-n}$, $C_w > 10^{-3}$ for "wet" olivine is the weight water concentration (in %%). It should be noted the constants in (7) vary considerably in the papers referred to by [13] and heretofore we gave averaged values of constants. At $C_w = 10^{-3}$ on accounting for

$$\tau_{ik}^{\ 2} = (4 \times \eta^2) \times [(\psi_{zz} - \psi_{xx})^2 / 2 + 2 \times \psi_{xz}^{\ 2}] \tag{8}$$

non-dimensional viscosity is

$$\eta = \{ 1.0 / [(\psi_{zz} - \psi_{xx})^2 / 2 + 2 \times \psi_{xz}^{\ 2}]^{1/3}\} \times \exp\{ [10.0 + 5.0 \times (1 - z)] / T \} \tag{9}$$

Following [13] we assume the phase functions $\Gamma^{(l)}$ as

$$\Gamma^{(l)} = (1/2)\times\{1 - th\, [\mathrm{z} - \mathrm{z}^{(l)}(T)] / w^{(l)}\};\ \mathrm{z}^{(l)}(T) = \mathrm{z}_o^{(l)} - \{[\gamma^{(l)} \times (T - T_o^{(l)})] / (\rho \times g)\} \tag{10}$$

where the signs are changed as z-axis is pointing upwards, $z^{(l)}(T)$ is the depth of the l-th phase transition (l = 410, 660), $z_o^{(l)}$ and $T_o^{(l)}$ are the averaged depth and temperature of the l-th phase transition, $\gamma^{(410)}$ = 3 MPa×K^{-1} and $\gamma^{(660)}$ = –3 MPa×K^{-1} are the slopes of the phase equilibrium curves, $w^{(l)}$ is the characteristic thickness of the l-th phase transition, $T_o^{(410)}$ =1800$^{\mathrm{o}}$ K, $T_o^{(660)}$=1950$^{\mathrm{o}}$ K are the mean phase transition temperatures. The heats of phase transitions are neglected in (2) as insignificant in the case of developed convection as in [13]. From (10) it follows

$$\Gamma_{\mathrm{x}}^{(l)} = - (\gamma^{(l)} / 2\times\rho\times g\times w^{(l)}) \times T_x \times ch^{-2}\{[(z - z_o^{(l)} + \gamma^{(l)} \times (T\text{-}T_o^{(l)})) / (\rho\times g)] / w^{(l)}\} \tag{11}$$

Where from it is clear the phase transition with $\gamma^{(l)} > 0$ facilitates convection (at l = 410), while the phase transition with $\gamma^{(l)} < 0$ hinders convection (at l = 660). In non-dimensional form $z_o^{(410)}$ = 0.38, $z_o^{(660)}$ = 0, $w^{(l)}$ = 0.05, $\gamma^{(410)}$ = 2.5×10^9, $\gamma^{(660)}$ = -2.5×10^9, $T_o^{(410)}$ = 0.92, $T_o^{(660)}$ = 1 and in (1)

$$\Gamma_x^{(l)} = -(\delta\cdot\rho^{(\lambda)}\gamma^{(l)}/2\times\rho\, Ra^{(l)}\times w^{(l)})\times T_x\times ch^{-2}\{[z - z_o^{(l)} + \gamma^{(l)}(\delta\rho^{(\lambda)}/\rho\cdot Ra^{(l)})\times(T\text{-}T_o^{(l)})] / w^{(l)}\} \tag{12}$$

Equations (1)–(2) are solved for the isothermal horizontal and vertical boundaries regarded no-slip impenetrable ones except for the "windows" for in- and outgoing subducting plate, where the plate velocity is specified. Vertical boundary distant from subduction zone is assumed penetrable at right angle; the latter boundary condition appears not too imposing in the case of very flat subduction. Q in (2) is non-zero in the continental and oceanic crust 40 and 7 *km* thick. Initial vertical boundaries temperature is calculated for the half-space cooling model for 10^9 yr and 10^8 yr for Euro-Asian (continental) plate and Apulian lithospheric microplate (paleooceanic plate) respectively. It is convenient to express dimensionless $\tau^2_{\iota\kappa}$ in (2) through the stream-function ψ as in (8):

$$\tau_{ik}^{\ 2} = (4 \times \eta^2) \times [(\psi_{zz} - \psi_{xx})^2 / 2 + 2 \times \psi_{xz}^{\ 2}]$$

III. RESULTS AND DISCUSSION

Assuming the heat flux maximum q is formed above the convective flow, upwelling towards the Pannonia basin and Vardar zone, and the convection cell dimension is equal to horizontal scale of the heat flux anomaly zone, the convection cell dimension can be estimated of ~ 300 km. To more accurately compute the consistent model of small-scale convection in the mantle wedge between the overriding Euro-Asian plate and subducting Apulian lithospheric microplate it is necessary from the computational point of view first to specify in (1)–(2) vanishing non-dimensional numbers $Ra\to0$, Di = 0, i.e. to ignore convection and viscous dissipation. This approach is applied as convection with Ra and Di (4) passes through rather vigorous stages, and the time steps in integrating (1)–(2) become too small thus making it difficult to model the thermal structure of the plates. Solving (1)–(2) by the finite element method in space on the grid 104×104 and the 3-rd order Runge-Kutta method in time one obtains for $Ra\to0$, Di = 0 and V=10 mm a year non-dimensional quasi steady-state ψ and T shown in fig. 1, where the streamlines are depicted with the step 5 and the isotherms with an interval 0.05.

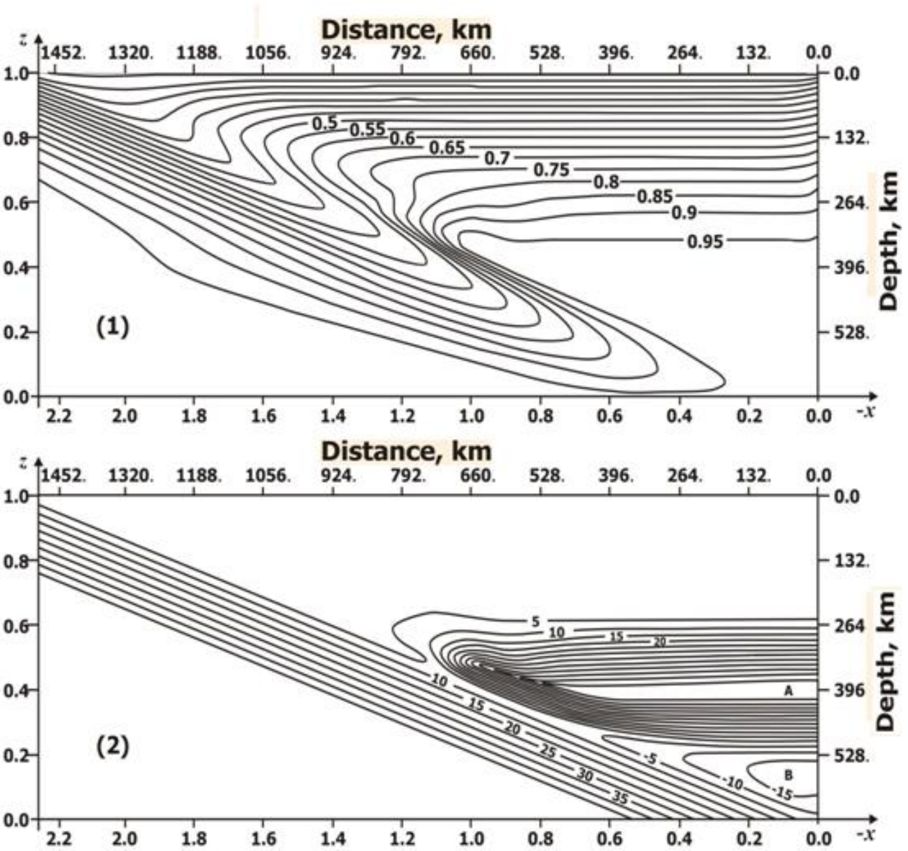

FIGURE 1. Schematic cross section of the region of subduction of the Apulian lithospheric microplate under the Euro-Asian plate with no effects of viscous dissipation and convection taken into account. (1) – the quasi steady-state distribution of non-dimensional temperature and (2) – the quasi steady-state distribution of stream-function, the streamlines above the subducting slab correspond to the mantle wedge flows ("A" and "B") induced by subduction.

Subducting plate was considered rigid, while the viscosity at the zone of plates friction (at temperatures below 1200^{o} K) was reduced by 2 orders of magnitude as compared to (7). The latter viscosity reduction at the plates contact zone accounts for lubrication effected by deposits partially entrained by the subducting plate. Such a lubrication prevents the overriding Euro-Asian plate from gluing to the subducting one [9]. Fig. 1 shows the results of computation for the formulae (7) – (9) for non-Newtonian rheology case for the water content $C_w = 3\times10^{-1}$ weight %. The velocity V=10 mm per year is chosen as resulting in the best fit of the model convective zone size to horizontal extent of the observed heat flux anomaly in Pannonia basin and the Vardar zone. The Apulian lithospheric microplate subducting with a given velocity V is considered rigid and is shown in Fig. 1(2) by the equidistant diagonal streamlines. The induced mantle wedge flow above the subducting plate is seen to occur in the form of two vortices A and B (located one above another), the latter 2 vortices being considerably compressed in the vertical direction and the upper one (with $\psi > 0$) revolves clockwise while the lower one (with $\psi < 0$) revolves counterclockwise. In Fig. 1(2) the upper induced flow "A" is seen to be firmly pressed to the subducting Apulian lithospheric microplate, the strain rate in the zone of contact of the opposite flows (i.e. flow "A" and subducting slab) being very high thus resulting in the viscosity (7) drop by several orders of magnitude. It should be noted that in the case of non-Newtonian rheology the greater the subduction angle the more extensive is this contact zone, in which the dissipative heat release mainly occurs. This may serve the reason why the Karig vortices (and the resulting back-arc spreading) are formed in the zones of comparatively steep subduction. The opposite flow "A" in Fig. 1(2) apparently is induced by the flow "B", forced by subducting plate.

Assuming $Ra = 5.55\times10^{8}$ and $Di = 0.165$, i.e. switching dissipation and convection on, taking into account the effects of phase transitions, from (1)–(2) the convection at $C_w = 3\times10^{-1}$ weight % is found to destroy the induced mantle flows in the mantle wedge during the time interval ~ 0.6×10^{-6} (in dimensional form ~ 0.1 Ma) and to assume the quasi steady-state form shown in Fig. 2, in which the streamlines in the convection vortices are depicted with the interval 4×10^{4}.

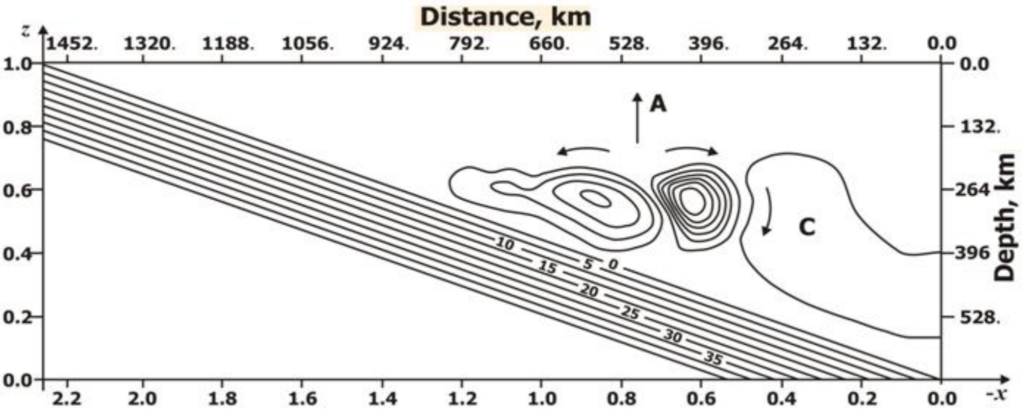

FIGURE 2. Quasi steady-state non-dimensional stream-function distribution in the zone of subduction of the Apulian lithospheric microplate under the Euro-Asian plate with the effects of dissipative heating and convection taken into account for non-Newtonian rheology for the water content C_w=3×10^{-1} weight %. Parallel equidistant streamlines represent subducting Apulian lithospheric microplate. Arrow "A" shows possible direction of the upward convective transport of dissipative heat and mantle hydrocarbons to the Earth's surface.

These convective vortices are seen actually to correspond to a single convection cell aroused at subduction velocity V = 10 mm×a^{-1}. The latter convection cell dimension is of the order of ~ 300 km, i.e. is very close to the observed horizontal extent of the heat flux anomaly observed in the Pannonia basin and Vardar zone. The velocity in convective vortices may exceed 10 m×a^{-1} for the water content of 3×10^{-1} weight %. The direction of a possible upward transport of mantle hydrocarbons and dissipative heat to the Earth's surface is shown by the arrow "A". It should be noted that in the case of Newtonian rheology the convection in the mantle wedge cannot be aroused at the velocity of subduction of 10 mm×a^{-1} and subduction angle of 25°.

In Fig. 3 the quasi steady-state stream-function ψ is shown for the mantle water content of 0.3×10^{-1} weight %, in which case the dissipation-driven convection is aroused in essentially a single vortex with a characteristic velocity of ~10 mm×a^{-1}.

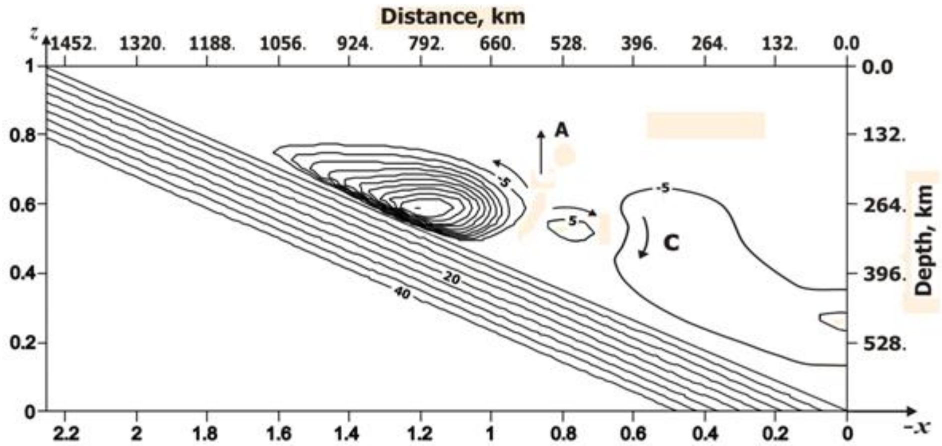

FIGURE 3. Quasi steady-state non-dimensional stream-function distribution in the zone of subduction of the Apulian lithospheric microplate under the Euro-Asian plate with the effects of dissipative heating and convection taken into account for non-Newtonian rheology for the water content C_w = 0.3×10^{-1} weight %. Parallel equidistant streamlines represent subducting Apulian lithospheric microplate. Arrow "A" shows possible direction of the upward convective transport of dissipative heat and mantle hydrocarbons to the Earth's surface.

This convective flow may serve a means of the upward mantle hydrocarbons and dissipative heat transport, which direction is shown in Fig. 3 by the arrow "A". Such a convective flow may cause the back-arc spreading in the Pannonia basin and the Vardar zone. At the mantle water content C_w < 0.3×10^{-1} weight percent the dissipation-driven convection cannot be aroused in the mantle wedge even in the case of the non-Newtonian rheology for subduction velocity of ~10 mm$\times a^{-1}$ and angle of 25°.

It is worth noting that in the case of Newtonian rheology the 2D transversal convective rolls in the mantle wedge, as in Fig. 2, can be formed only at sufficiently small angles of subduction. Thus, at β = 30° the transversal convective rolls are not formed even at the velocity of subduction of 100 mm$\times a^{-1}$ [5, 9]. In the case of the non-Newtonian rheology the transversal rolls (2D Karig vortices) can be aroused at greater subduction angles and sufficiently small subduction velocities owing to viscous friction in the zone of contact of the opposite induced flow ("A" in Fig. 1) and subducting slab. It should be noted that numerous thermo-mechanical mantle models in the zones of subduction (see, e.g. [8, 9] and the vast number of references there) showed convection in the form of transversal rolls never to occurred as the models with extremely small subduction angle and sufficiently great subduction velocity were not investigated.

IV. CONCLUSION

The size of the cell of 2D mantle wedge dissipation-driven convection in the case of the realistic non-Newtonian rheology equals ~ 300 km at the subduction velocity 10 mm$\times a^{-1}$, in which case a single convection cell is aroused. This explains the formation and horizontal extent of the only 2D heat flux anomaly observed in the rear of the Dinarides. The water content sufficient for the 2D convection to be aroused is ~ 3×10^{-1} weight %, or, alternatively, it is ~3×10^{-2} weight %, but the 2D convection is aroused as a single Karig vortex. The velocity in convective vortices in the non-Newtonian rheology case is ~10 m per year at the water content C_w ~ 3×10^{-1} weight percent and □ 10 mm per year at the water content C_w ~ 0.3×10^{-1} weight percent in the mantle wedge. The upwelling convective flow may be sufficient to provide upward transport of mantle wedge hydrocarbons to the Earth's surface.

REFERENCES

[1] D. Babbicci, C. Tamburelli, M. Viti, E. Mantovani, D. Albarello, F. D'Onza, N. Cenni, E. Mugnaioli, "Relative motion of the Adriatic with respect to the confining plates: seismological and geodetic constraints", Geophys. J. Int., vol. 159, pp. 765 – 775, 2004.

[2] M. Billen, G. Hirth, "Newtonian versus non-Newtonian Upper Mantle Viscosity: Implications for Subduction Initiation", Geophys. Res. Lett., vol. 32, (L19304), 2005, Doi:10.1029/2005GL023458.

[3] E. Carminati, M. Lustrino, C. Doglioni, "Geodynamic evolution of the central and western Mediterranean: Tectonics vs. igneous petrology constraints", Tectonophysics, vol. 579, pp. 173 – 192, 2012.

[4] S.V. Gavrilov, "Investigation of the island arc formation mechanism and the back-arc lithosphere spreading", Geofizicheskie Issledovaniya, vol. 15 (4), pp. 35–43, 2014.

[5] S.V. Gavrilov, D.H. Abbott, "Thermo-mechanical model of heat- and mass-transfer in the vicinity of subduction zone", Physics of the Earth, vol. 35, pp. 967–976, 1999.

[6] S.V. Gavrilov, A.L. Kharitonov, "Velocity of the subduction of the Russian platform under the Siberian one in the Paleozoic by the distribution of mantle hydro-carbon upwelling zones in Western Siberia", Geofizicheskie Issledovaniya, vol. 16, pp. 36–40, 2015.

[7] S.V. Gavrilov, A.L. Kharitonov, "Subduction velocity of the Russian plate under the Siberian one at Paleozoic: a constraint based on the mantle wedge convection model and the oil- and gas-bearing zones distribution in Western Siberia", Modern Science, vol. 16, pp. 155-160, 2016.

[8] T.V. Gerya, J.A.D. Connolly, D.A. Yuen, W. Gorczyk, A.M. Capel, "Seismic implications of mantle wedge plumes", Phys. Earth Planet Interior, vol. 156, pp. 59-74, 2006.

[9] T.V. Gerya, "Future directions in subduction modeling", J. of Geodynamics, vol. 52, pp. 344-378, 2011.

[10] L. Lenkey, P. Dovenyi, F. Horvath, "Cloetingh Geothermics of the Pannonian basin and its bearing on the neotectonics", EGU Stephan Mueller Special Publication Series, N. 3, pp. 29 – 40, 2002.

[11] L.H. Royden, F. Horvath, A. Nagymarosy, L. Stegena, "Evolution of the Pannonian basin system: 2. Subsidence and thermal history", Tectonics, N. 2, pp. 91 – 137, 1983.

[12] G. Schubert, D. L. Turcotte, P. Olson, "Mantle Convection in the Earth and Planets", New York, Cambridge University Press, 940 p., 2001.

[13] V.P. Trubutsyn, A.P. Trubitsyn, "Numerical model of formation of the set of lithospheric plates and their penetration through the 660 km boundary", Fizika Zemli, N. 6, pp. 138 - 147, 2014.

[14] V.N. Zharkov, "Geophysical Researches of the Planets and Satellites", Moscow: Joint Institute of Physics of the Earth RAS, 102 p., 2003.

[15] V.N. Zharkov, "Physics of the Earth's Interiors", Moscow: Nauka i obrazovanie, 384 p., 2012.

Mechanical Characterization of two Amorphous Polymers in Traction-Compression Test using A Viscoelasticimeter

Ayarema AFIO[1], Komlan LOLO[1], Komlan Assogba KASSEGNE[1], Yaovi Ouézou AZOUMA[2], Emmanuel FOLTETE[3]

[1]University of Lome, Ecole Nationale Superieured' Ingénieurs (ENSI) / Department of Mechanical Engineering, 01 BP 1515 Lomé 01, Togo

[2]University of Lome, School of Agronomy / Department of Rural Engineering and Agricultural Machinery, 01 BP 1515 Lomé 01, Togo

[3]University of Franche-Comté, FEMTO ST Institute, UMR CNRS 6174, Department of Applied Mechanics, 24 rue de l'Épitaphe F-25000 Besançon, France

Abstract— *Using the viscoelasticimetric tests in traction and compression mode, the viscoelastic sizes E', E" and tanδ were characterized according to the temperature and this, for amorphous polymer samples differentiated by their fluidity index. It is noted that the stiffness is intermediate size making it possible to characterize the conservative components E' easily and the dissipative one E" of the module complexes E* like its temperature of glass (vitreous) transition from polymer trough the factor of loss tanδ. These sizes in comparison with the abundant data by the manufacturers make it possible to consolidate the mode of request retained:*

- *The temperature of vitreous transition Tg obtained on the two samples from methylpolymethacrylate (PMMA) in modetraction compression is integrated in the interval of temperatures (110 to 135°C) advised by the manufacturers of this material.*
- *The ranks of polycarbonate (PC) tested in the two modes had a constancy of behaviour with Tg quasi equivalent to150°C with a variation of 5°C.*

Keywords— ***amorphous polymer, viscoelacticimetry, temperature, vitreous transition.***

I. INTRODUCTION

The behavior of polymeric materials, by taking temperature as a descriptive variable of their hierarchization, makes it possible to specify in particular the domain of their specific properties which concern:

- The solid-state viscoelastic materials associated with the notion of rigid-rubber transition,
- The more intuitively characteristic flows of a viscous liquid state.

These two aspects define the rheological behavior of these materials and we simply recall that rheology is, as a first approach, the science that studies the evolution of the deformation and flow of condensed phases under imposed stress. In practice, the dependent parameter may be in addition to the temperature, the deformation or the rate of deformation.

In addition, pasty solid-solid, solid-solid, viscous solid, viscous-liquid solid, solid-liquid, liquid-liquid solid passages are sometimes difficult to apprehend. This is explained by the fact that these different state phases are sometimes a function of the temperature of the test, the mode of loading and the time of application.

The range of reference temperatures that make it possible to qualify the evolutions of polymer materials via thermal experimental references mainly comprises [1-16], [26]:

- The glass transition temperature;
- The Vicat softening temperature;
- The Martens temperature;
- The embrittlement temperature;
- The temperature of deflection under load;
- The liquid-liquid transition temperature;
- The freezing temperature;

- The melting temperature in the case of semi-crystalline polymers.

On this basis, it was envisaged to carry out a structured study concerning a contribution to the qualification of the rheology of different amorphous polymeric materials: polymethylmethacrylate (PMMA), polycarbonate (PC), polyetherimide (PEI), materials selected for their practical applications.

General laws of rheological behavior can in fact be released without involving molecular approaches complementary to these descriptive approaches.

To qualify the linear viscoelastic behavior of polymeric materials [2, 4, 6, 17-19], recalling classically that these materials have an intermediate behavior between that of an elastic solid obeying the Hooke's law (or in shear to the relation) and that of a viscous liquid described by Newton's law (that is to say the relation $\tau = \eta\ (\gamma)^{\cdot}$ [3, 6, 10, 12, 20, 21].) We opted to conduct experiments in dynamic mode at using tensile-compression type tests using a viscoelasticimeter, in order to determine the dynamic quantities in terms of complex modulus, of loss factor, with the aim of achieving a hierarchy of observed behaviors.

The resulting representations are of the type: Modules (dissipative or conservative) function of the temperature f (T).

The apparatus, which in principle can be considered as a "capillary rheometer", has been used by imposing different loads on the material so as to obtain experimental data which can be presented in the form of rheograms:

$$\tau = f(\dot{\gamma}) \tag{1}$$

It is on this basis that the work carried out has been implemented paying particular attention to:

a) In the first place to the experimental determination of the characteristic temperatures and following different complementary approaches.

The variability or the conservatively of these data being associated with the different selected materials ranked in first approach according to the value of their melt index.

b) In the second place to the rheological evolutions of the polymers taken as model of behavior, and this according to an apparatus currently or not used for these determinations.

The originality of the chosen approach concerns the different geometrical configurations that are sometimes non-standard and their extrapolation makes it possible to obtain descriptive rheograms of the properties of use.

II. MATERIAL AND METHOD

2.1 Material

The device used at the Laboratory of Surface Microanalysis (LMS) was a visco-analyzer brand Metravib. (Fig. 2) schematizes the various functional components of the apparatus which are:

- A frequency exciter operating in the range 7.8 - 1000 Hz,
- A displacement sensor which directly measures the displacement for the frequency selected for the tests,
- A force sensor,
- A phasemeter calculating and displaying the phase difference between the signals supplied by the displacement sensor and those originating from the force sensor,
- An amplifier which filters, amplifies and converts the displacement and force signals into proportional DC voltages so as to allow direct display of the stiffness,
- A temperature regulator of the enclosure in which the sample is positioned.

Practically one imposes for a frequency of stress, an initial deformation, as well as the amplitude of deformation on both sides of the imposed value.

The experimental variable is the temperature selected in the range [20; 200 ° C] for the amorphous materials retained in this work.

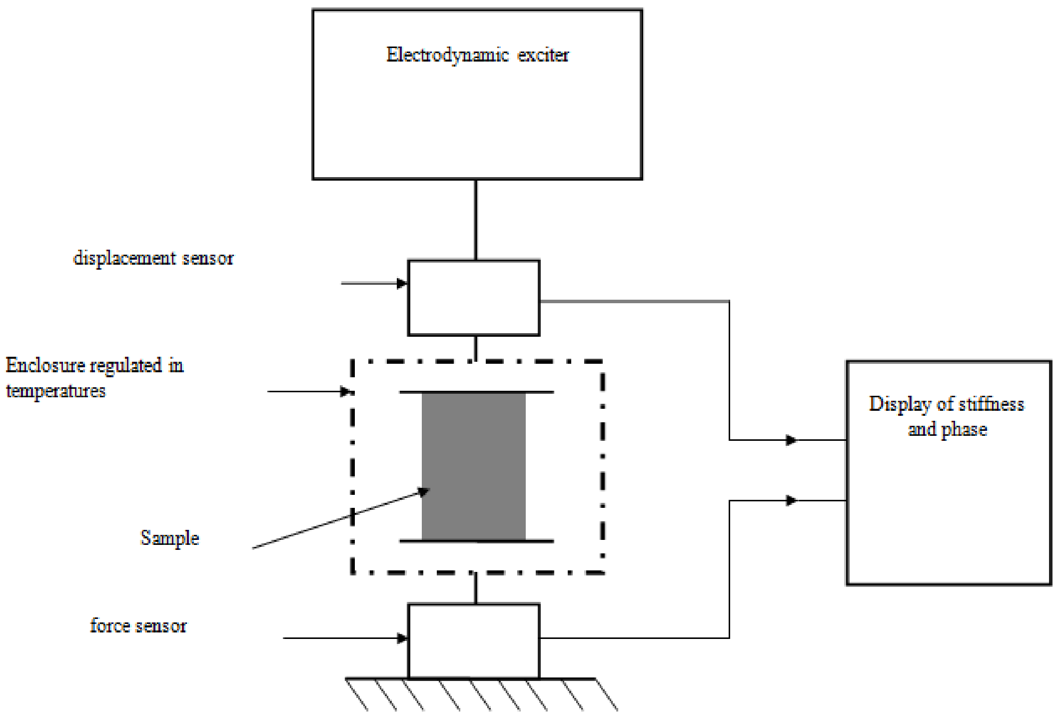

FIGURE 1: Schematic representation of the visco-analyzer metavib principle [7, 22]

The massive sample of defined geometry (parallelepiped or cylinder) is positioned by gluing between two trays of the sample holder (see Figure 1).

2.2. Method

The materials selected for this work, PMMA amorphous polymers and PC, were selected from the polymers that we studied in our PhD work [26].

Samples of tested materials are shaped by cutting into polymer sheets.

We deduce the values associated with the notions of:

- excited surface (Se = π R2 case of the cylinder, Se = L x l case of the parallelepiped, R being the radius, L and l being respectively the length and the width),
- free surface (Sl = 2π R H case of the cylinder, Sl = 2 H (L + l) case of the parallelepiped), if H is the height of the cylinder or the parallelepiped,

Which make it possible to apprehend the value of the form factor [18, 20].

$$f_c = \frac{1}{1+2\left[\frac{S_e}{S_l}\right]^2} \tag{1}$$

To overcome the correction, we seek a corrective factor equal to unity. Most often one selects L = 20 mm, l = 10 mm, H = 20 mm, R = 5 mm,

Which gives:

Se = 40 mm ^{2} and Sl = 600 mm ^{2}, ie fc = 0.996 for the parallelepiped, and

Se = 78.5 mm ^{2}, Sl = 314 mm ^{2}, ie fc = 0.89 for the cylinder.

Several works [1, 4, 5, 10-13] have shown that from the stiffness k, a non-conservative size of a material, one can model its elastic and viscoelastic properties.

Generally, the quantification of k is determined by making the ratio of the applied force (ΔF) to the associated displacement (Δx):

$k = \frac{\Delta F}{\Delta x}$,k expressed in g.μm^{-1} or in N.m^{-1}

Stiffness metrology, which is a Young's modulus-related quantity E for a constant sample geometry $k = \frac{ES}{L}$ where S and L are characteristics of the geometry of the sample), is often carried out via the following mechanical test methods: compression, tension, shear, bending, buckling or torsion [14] [15].

A corrective factor fc is associated with k to take into account the so-called lateral deformation in the sample [3]:

$$k = f_c \cdot E \frac{S}{L} \tag{3}$$

Since, with the chosen test apparatus, we work in dynamic mode, the notion of dynamic stiffness k* is introduced by expressing:

$$\left|k^*\right| = \left|\frac{F(t)}{x(t)}\right| = f_c E^* . \frac{S}{L} = k' + i\, k'' \tag{4}$$

The final expression of k*, just like that of the dynamic complex module E* = E'+ i E', is dependent on the rheological model selected to describe the behavior of the material.

It is recalled that k ', E' respectively correspond to the stiffness and the conservative module, and k '', E '' are associated with the dissipative quantities of the stiffness and the complex modulus.

III. RESULTS AND DISCUSSION

Different rheological models combining springs and dampers make it possible to describe the viscoelastic behavior of materials [1, 5, 10, 12, 17] and we will not recall for the record that the results are associated with the Kelvin-Voigt model.

This conventional model consists of a spring and a damper of characteristic η in parallel circuit, both subjected to a force F (t) generating a deformation ε (t) resulting from the displacement x (t) caused. The descriptive constraint of the Kelvin-Voigt model is written:

$$\sigma(t) = E\, \varepsilon\,(t) + \eta \frac{d\varepsilon(t)}{dt} \tag{5}$$

The complex quantities F * and x * associated with the values of F (t) and x (t) are such that [5, 7, 13, 18-20]

$$F^* = k \cdot x^* + \eta \frac{S}{L} \frac{dx^*}{dt} \tag{6}$$

The complex quantities F * and x * associated with the values of F (t) and x (t) are such that [5, 7, 13, 18-20]

$$k^* = k\left[1 + \eta \frac{S}{L} \frac{i\omega}{k}\right]$$

$$k_{dyn} = \left|k^*\right| = k\sqrt{1 + \frac{\omega^2}{k^2}\left(\eta \frac{S}{L}\right)^2} \tag{7}$$

Expression that one writes fluently according to the loss factor tanδ :

$$k_{dyn} = k\sqrt{1 + \tan^2 \delta} \;> k_{stat}$$

From the expression of k * we can go back to the dynamic module E *.

$$\begin{cases} E' = k'\dfrac{L}{S} = k\dfrac{L}{S}\cos\delta \\ E'' = k''\dfrac{L}{S} = k\dfrac{L}{S}\sin\delta \\ \tan\delta = \dfrac{E''}{E'} = \dfrac{k''}{k'} \end{cases} \tag{8}$$

These expressions do not take into account the form factor fc.

From a practical point of view, it is recalled that the equipment used gives for a given geometry of samples (S and L), values of k and δ.

3.1 Fractional Derivative Models [3, 19, 21] [7]

The mathematical tool associated with the fractional derivation is based on the introduction of an operator, the derivative of order a with respect to the time t($D_t^\alpha = \dfrac{d^\alpha}{dt^\alpha}$ with 0 <α <1), in writing the equations governing the associated rheological models.

In the case of the Kelvin-Voigt model, the classical expression of σ (t) written in the form

$$\sigma(t) = E\,\varepsilon(t) + \eta\frac{d\varepsilon(t)}{dt} \text{ becomes : } \sigma(t) = ED_t^\alpha\varepsilon(t) + \eta D_t^\alpha\varepsilon(t) \tag{9}$$

D_t^α is called fractional derivative with $0 \le \alpha \le 1$

For a viscoelastic material described by the fractional model of Kelvin-Voigt we have:

$$T\,F\left[D_t^\alpha\sigma(t)\right] = [E + \eta(i\omega)^\alpha]TF\left[\varepsilon(t)\right] = E^*\ TF\left[\varepsilon(t)\right] \tag{10}$$

Since it is shows that the Fourier transform of D_t^α f(t) is written:

$$TF\left[D_t^\alpha f(t)\right] = (i\omega)^\alpha TF\left[f(t)\right] \tag{11}$$

This method used in the thesis of MARTIN C. [7] allows in particular to easily apprehend the value of δ.

3.2 Results and discussion

The work yielded numerical data which led to the representative curves of the modules E '(T), E "(T) and the loss factor tanδ (T). They describe the dynamic behavior of the different classes of polymeric materials, selected according to their differentiated melt index are shown in Figures 3 to 5 and in Table 1.

The following comments may be associated with them:

a) For polymethyl methacrylate (PMMA) material, it is noted (see Figures 2 to 4):

A decrease in the conservative (E ') and dissipative (E ") modules as a function of the increase in the melt index, which results in a decrease in the dynamic modulus as a function of the increase in the value of this index (see Table 1),

A measurable variation of the glass transition temperature determined in dynamic mode for the two melt flow indices selected.

b) These modifications observed on the amplitudes of the modules and the descriptive temperatures of the viscoelastic behavior are found on the material polycarbonate (PC) by noting that (see figures 5 to 7) and table 1:

The variation calculated directly on the complex module remains of the order of 10%; the variation of the glass transition temperature noted is 5°C.

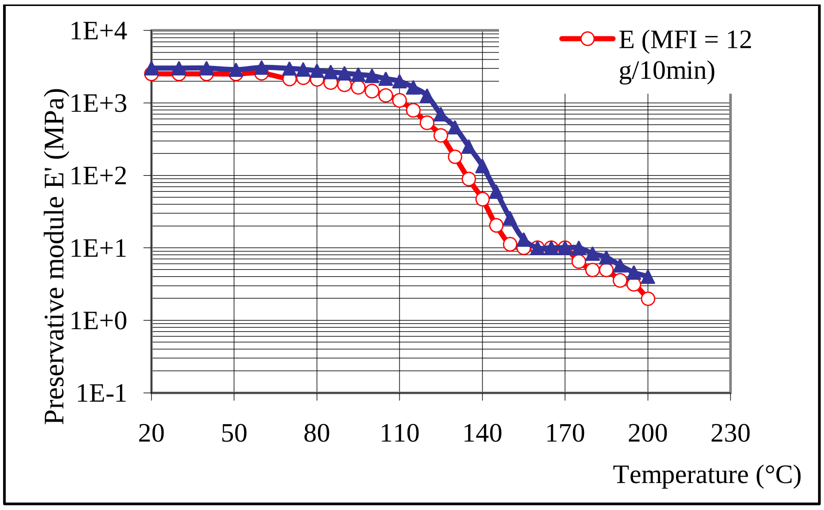

FIGURE 2: Conservative module E 'of polymethyl methacrylate (PMMA) characterized by differentiated fluidity indices, tested in dynamic traction-compression mode.

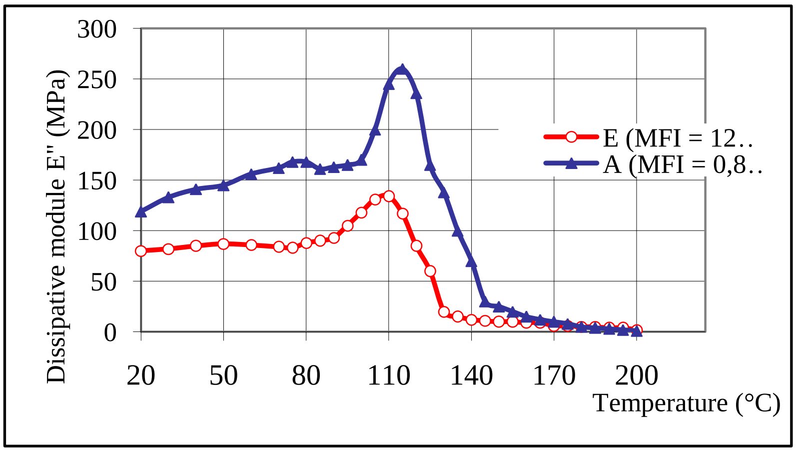

FIGURE 3: Dissipative module E "of polymethylmethacrylate characterized by differentiated melt indexes, tested in dynamic traction-compression mode

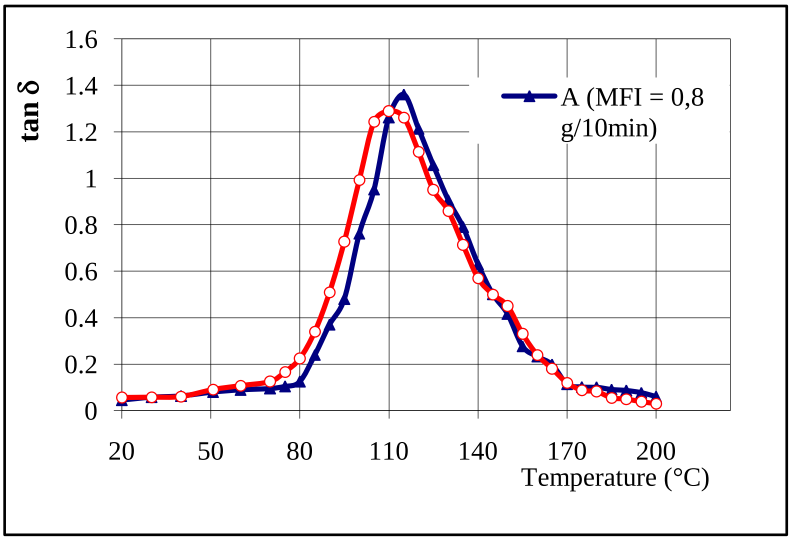

FIGURE 4: Polymethyl methacrylate tanδ loss factor characterized by differential fluidity indices, tested in dynamic traction-compression mode

TABLE 1
VALUES OF THE COMPLEX DYNAMIC MODULUS E * AND OF THE GLASS TRANSITION TEMPERATURE IN TRACTION-COMPRESSION TYPE DYNAMIC MODE.

Materials	Melt Flow Index MFI (g/10min)	dynamic module E* (MPa) (20°C)	Vitreous (Glass) transition Temperature measured T_g (°C)
PMMA	0,8	3020	115
	12	2510	110
PC	10	2250	150
	17,5	2000	145

From the experimental results, we can observe the following graphics of the preservative module E'.

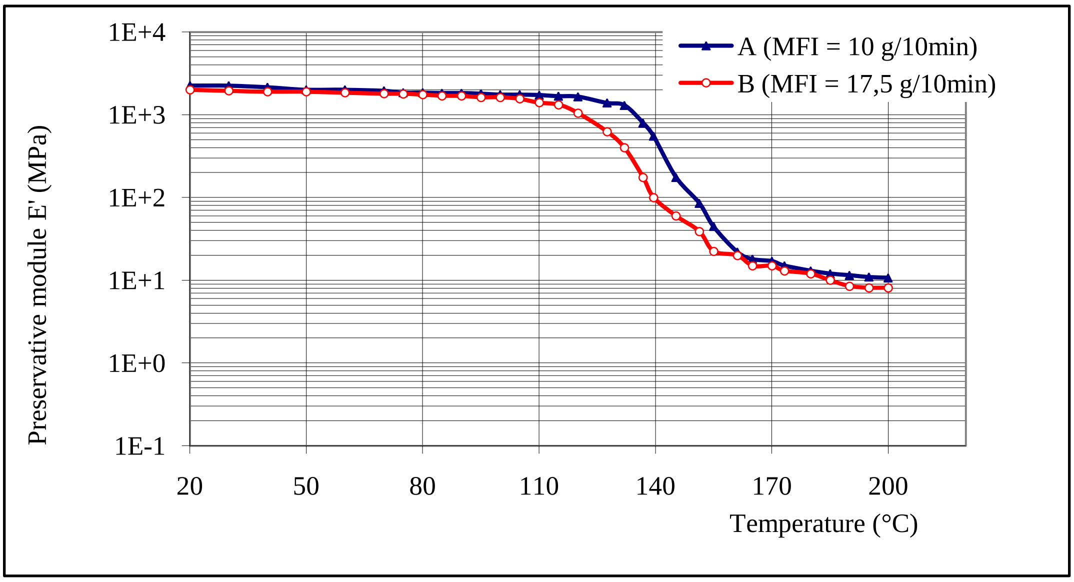

FIGURE 5: Preservative module E 'of polycarbonate characterized by differentiated fluidity indices and tested in dynamic traction-compression mode.

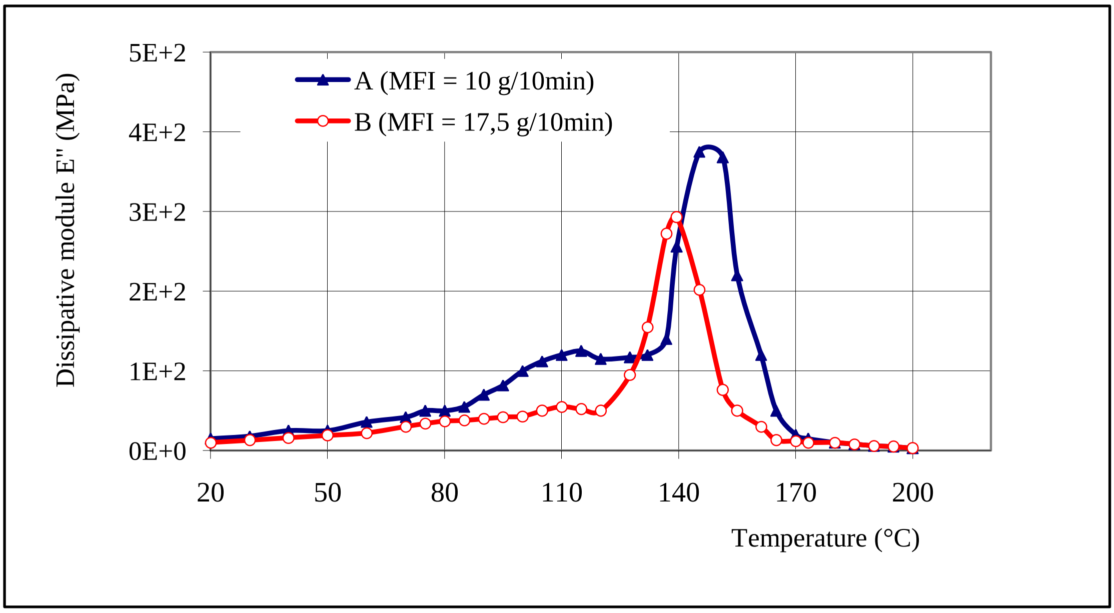

FIGURE 6: Dissipative module E" of Polycarbonate characterized by differentiated fluidity indices and tested in dynamic traction-compression mode

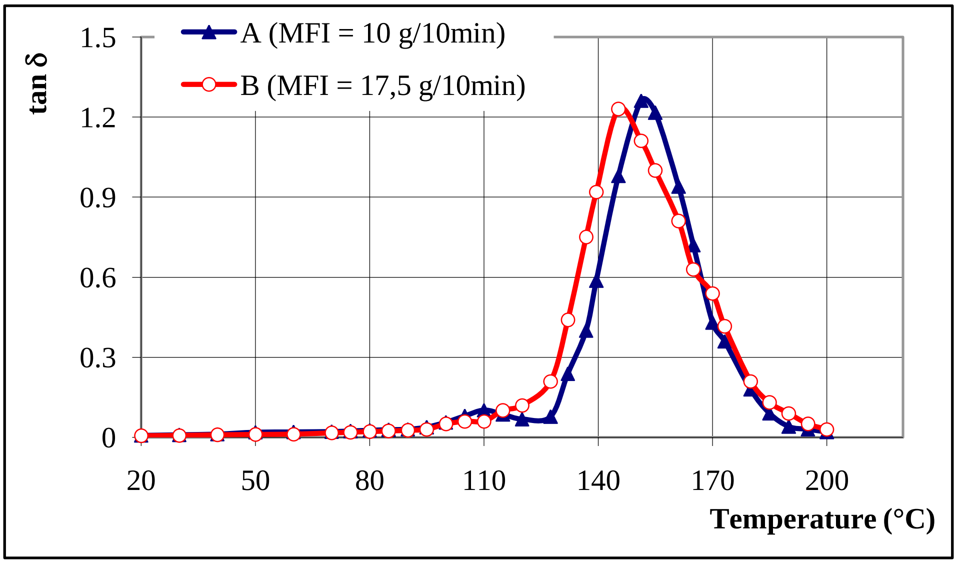

FIGURE 7: Loss factor tanδ of polycarbonate characterized by differentiated fluidity indices and tested in dynamic traction – compression mode.

However, the change in the melt index even in a factor of 4 does not have any effect on the value of the glass transition temperature.

IV. CONCLUSION

The representation of the different viscoelastic quantities (E ', E ", tanδ) of each material as a function of temperature (see Fig. 3 to 8) made it possible to differentiate the behavior of the polymers of distinct melt index.

For all the results obtained by the tensile-compression mode tests on the different amorphous polymers (PMMA, PC), it was found that the evolution of the loss factor tanδ qualifying the glass transition temperature (Tg) by a maximum peak has been used to record Tg supporting the theoretical data provided in the technical brochures and in the literature [1, 4, 10, 21, 23].

The values recorded could be associated with the Vicat softening temperatures of the material.

In a global way, the variation of the conservative modulus E '= f (T) allowed, whatever the material tested in traction - compression mode, to identify three domains of behavior:

- elastic-vitreous where the rigidity of the polymer is observed,
- viscoelastic in which the amplitude of E "and the Tg are recorded,
- elastic - rubbery.

REFERENCES

[1] **J. J. AKLONIS et W. J. MACKNIGHT**, "Introduction to polymer viscoelasticity", Ed. John Wiley, 1979.

[2] **J. P. ANDRE**, "Les moyens de mesure des caractéristiques des matériaux viscoélastiques", Revue de Chimie Actualité, 1980.

[3] **F. BUECHE**, "Viscoelasticity of polymethacrylates", Journal of applied physics, vol. 26 n° 6, 1955.

[4] **R. M. CHRISTENSEN**, "Theory of viscoelasticity - an introduction", Ed. Academic Press, 1982.

[5] **J. D. FERRY**, "Viscoelasticity properties of polymers", Ed. John Wiley, 1980.

[6] **J. F. MAY**, "Viscosité et viscoélasticité des polymères fondus : exploitation des résultats de mesure", Technique de l'ingénieur, vol. AM3 n° A3616, 1990.

[7] **C. MARTIN**, "Intérêt de la dérivation fractionnaire pour une théorie unifiée de la viscoélasticité des matériaux", thèse de l'Université de Franche Comté, 1999

[8] **H. E. MASRI**, "Qualification des propriétés viscoélastiques de classes des matériaux sélectionnés en fonction de leur propriétés d'adhérence", thèse de l'université de Franche Comté, 1992

[9] **N. W. TSCHOEGL**, "Phenomenological theory of linear viscoelasticity behavior", Ed. Springer, 1989.

[10] **W. J. FREEMAN, C. K. SCHOFF et A. R. COOPER**, "Polymers : polymer characterization and analysis. Encyclopedia reprint series", Ed. John Wiley & Sons, Wiley interscience, 1992.

[11] **D. FROELICH**, "Viscoélasticité des polymères", JFP, pp. 29 - 86.

[12] **J. L. CHABOCHE et J. L. MAITRE**, "Mécanique des matériaux solides", Ed. Dunod, 1988.

[13] **T. BEDA**, "Module complexe des matériaux viscoélastiques par essais dynamiques sur tiges ; petites et grandes déformations", thèse de CNAM Paris, 1990

[14] **A. AFIO**, "Etude de comportement des matériaux composites par le test de torsion gauchissante," DEA, Science des matériaux, mécanique et mécanique des surfaces, Université de Franche Comté, 1996.

[15] **B. GARNIER**, "Isolation antivibratoire et antichoc - solutions technologiques et industrielles", Technique de l'Ingénieur, vol. AM3, pp. B5141-1 à B5142-2, 1990.

[16] **J. F. MAY**, "Viscoélasticité des polymères à l'état fondu. Rhéométrie en régime dynamique", Technique de l'ingénieur, vol. AM3 n° A3617, 1985.

[17] **P. HAMELIN**, "Contribution à l'étude du comportement rhéologique de liants viscoélastiques en vue de l'analyse du fluage des matériaux composites utilisés sous forme de structures en génie civil.", thèse de Doctorat d'Etat de l'université Claude Bernard - Lyon I, 1979

[18] **R. L. BAGLEY**, "Thermorheologically complex materials", International journal of engineering science, vol. 29, pp. 797 - 806, 1991.

[19] **A. FAGES**, "Modélisation du comportement des matériaux viscoélastiques par une méthode de dérivation fractionnaire", Matériaux et Techniques, vol. 12, pp. 23-30, 1993.

[20] **A. R. PAYNE**, "Shape factors and functions in rubber engineering", The engineer, vol. vol. 207, pp. 368 - 370, 1959.

[21] **B. READ et D. G. DEAN**, "The determination of dynamic properties of polymers and composites", Ed. Adam Hilger LTD, 1978.

[22] **A. JOUANDEAU, M. SALVIA, B. DUPERRAY, et al.**, "Estimation sur échantillons du comportement dynamique de grosses pièces en élastomères chargées", Matériaux et Techniques, pp. 255-266, 1982.

[23] **G. CHRETIEN et D. HATAT**, "Initiation aux plastiques et aux composites", Ed. Lavoisier, Tec & Doc, 1990.

[24] **M. ALBIGES et A. COIN**, "Résistance des matériaux appliquée", Ed. Eyrolles, 1986.

[25] **A. BAZERGUI et al.**, "Résistance des matériaux", Ed. de l'Ecole polytechniques de Montréal, 1999.

[26] **A. AFIO**, "Contribution expérimentale à la rhéologie des polymèresenvued'applicationspratiques et industrielles", Thèse de l'Université de FrancheComté, Besançon, 2001.

AD Publications

Sector-3, MP Nagar, Bikaner,
Rajasthan, India
www.adpublications.org, info@adpublications.org